

The Importance of Lake Emergent Aquatic Vegetation for Estimating Arctic-Boreal Methane Emissions

Ethan D. Kyzivat¹, Laurence C. Smith¹, Fenix Garcia-Tigreros², Chang Huang^{1,3}, Chao Wang⁴, Theodore Langhorst⁴, Jessica V. Fayne⁵, Merritt E. Harlan⁶, Yuta Ishitsuka⁶, Dongmei Feng¹⁰, Wayana Dolan⁴, Lincoln H Pitcher^{5,8}, Kimberly P. Wickland⁷, Mark M. Dornblaser⁷, Robert G. Striegl⁷, Tamlin M. Pavelsky⁴, David E. Butman^{2,9}, and Colin J. Gleason⁶

¹Department of Earth, Environmental & Planetary Sciences and Institute at Brown for Environment & Society, Brown University, Providence, RI, 02912 USA

²School of Environmental and Forest Sciences, University of Washington, Seattle, WA, 98195 USA

³School of Urban and Environmental Sciences, Northwest University, Xi'an, Shaanxi, 710127 China

⁴Department of Earth, Marine and Environmental Sciences, University of North Carolina, Chapel Hill, NC, 27599 USA

⁵Department of Geography, University of California-Los Angeles, Los Angeles, CA, 90095 USA

⁶Department of Civil and Environmental Engineering, University of Massachusetts, Amherst, MA, 01003 USA

⁷Water Resources Mission Area, U.S. Geological Survey, Boulder, CO, 80303 USA

⁸Cooperative Institute for Research in Environmental Sciences (CIRES). University of Colorado, Boulder. Boulder, CO, 80309, USA.

⁹School of Engineering and Environmental Sciences, University of Washington, Seattle, WA, 98195 US

¹⁰Department of Chemical and Environmental Engineering, University of Cincinnati, OH, 45221 USA

Corresponding author: Ethan D. Kyzivat (ethan.kyzivat@aya.yale.edu)

Key Points:

- We provide a first quantification of emergent vegetation area across 4,572 lakes in four Arctic-boreal study areas using airborne mapping.
- Lake emergent vegetation coverage varies regionally from 1 to 59 percent of lake area and seasonally to a lesser degree.
- Accounting for this coverage could increase Arctic-boreal lake methane upscaling estimates by 21 percent.

36 **Abstract**

37 Areas of lakes that support emergent aquatic vegetation emit disproportionately more methane
38 than open water but are under-represented in upscaled estimates of lake greenhouse gas
39 emissions. These shallow areas are typically less than ~1.5 m deep and can be estimated through
40 synthetic aperture radar (SAR) mapping. To assess the importance of lake emergent vegetation
41 (LEV) zones to landscape-scale methane emissions, we combine airborne SAR mapping with
42 field measurements of vegetated and open-water methane flux. First, we use Uninhabited Aerial
43 Vehicle SAR (UAVSAR) data from the NASA Arctic-Boreal Vulnerability Experiment
44 (ABoVE) to map LEV in 4,572 lakes across four Arctic-boreal study areas and find they
45 comprise ~16% of lake area, exceeding previous estimates, and exhibiting strong regional
46 differences (averaging 59 [50–68]%, 22 [20-25]%, 1.0 [0.8-1.2]%, and 7.0 [5.0-12]% for the
47 Peace-Athabasca Delta, Yukon Flats, and northern and southern Canadian Shield areas,
48 respectively). Next, we account for these vegetated areas through a simple upscaling exercise
49 using paired methane fluxes from regions of open water and LEV. After excluding vegetated
50 areas that may already be accounted for as wetlands, we find that inclusion of LEV increases
51 overall lake emissions by 21 [18-25]% relative to estimates that do not differentiate lake zones.
52 While LEV zones are proportionately greater in small lakes, this relationship is weak and varies
53 regionally, underscoring the need for methane-relevant remote sensing measurements of lake
54 zones and a consistent criterion for distinguishing wetlands. Finally, Arctic-boreal lake methane
55 upscaling estimates can be improved with more measurements from all lake zones.

56

57 **Plain Language Summary**

58 Lakes are one of the largest natural sources of the greenhouse gas methane and are especially
59 common in high latitudes. Shallow, near-shore areas of lakes having emergent aquatic vegetation
60 emit disproportionately more methane than open water areas but are under-represented in broad-
61 scale estimates of lake greenhouse gas emissions. While lake depths are difficult to map from
62 remote sensing, emergent vegetation, which typically grows in water less than ~ 1.5 m deep, can
63 be detected via radar remote sensing. To assess the importance of these areas to landscape-scale
64 methane emissions, we combine airborne radar mapping with field measurements of vegetated
65 and open-water methane emissions. Zones of emergent vegetation vary regionally and comprise
66 ~16% of lake area on average. A simple estimate that accounts for both open water and emergent
67 vegetation methane emissions results in 21% increased overall lake methane emissions estimates.
68 Emergent aquatic vegetation coverage has only a weak relationship with lake size, making it
69 hard to predict. Therefore, to better estimate broad-scale methane emissions, we suggest using
70 remote sensing to create lake vegetation distribution maps and measuring methane emissions
71 from both vegetated and open water zones within lakes.

72

73 **1 Introduction**

74 Inland waters are the single largest natural source of the greenhouse gas methane (CH₄)
75 (Saunois et al., 2020; Wik, et al., 2016a). Lakes are estimated to be responsible for ~24% of all
76 inland water emissions, second only to wetlands (Bastviken et al., 2011; Saunois et al., 2020).
77 They emit methane via diverse pathways of diffusion, ebullition, transport through aquatic plant

78 tissue, and through a storage flux during turnover and/or ice melt in stratified lakes. Emissions
79 are strongly dependent on temperature, sediment carbon content, redox environment, and gas
80 transfer velocity (Bastviken, Cole, Pace, & Tranvik, 2004; Wik et al., 2016). Uncertainties in
81 upscaling lake emissions therefore have vast spatial and temporal heterogeneities (Loken et al.,
82 2019; Natchimuthu et al., 2016; Stephanie et al., 2020; Saunois et al., 2020).

83 Unlike for wetlands, there are few process-based models for lake fluxes, so estimates
84 have relied on data-driven extrapolations (Saunois et al., 2020). Lake emission upscaling efforts
85 have only recently begun to account for lake surface area (DelSontro et al., 2016; Hastie et al.,
86 2018; Holgerson & Raymond, 2016), but it is still rare to consider other aspects of morphometry,
87 such as slope, vegetation, and littoral area (Casas-Ruiz et al., 2021). “Bottom-up,” or process-
88 based, methane estimates tend to over-predict aquatic methane fluxes compared to “top-down,”
89 or inversion-based, models (Saunois et al., 2020), and double-counting of small lakes as
90 wetlands caused by mismatch in scale and methods among datasets has been suggested as a
91 possible cause (Thornton et al., 2016). Small ($< 0.001 \text{ km}^2$) lakes and wetlands are poorly
92 mapped, especially in Arctic-boreal regions containing the world’s greatest abundance of lakes
93 (Verpoorter et al., 2014). Indeed, uncertainty in wetland extent is frequently cited as the leading
94 cause of uncertainty in bottom-up methane estimates (Zhang et al. 2017), and errors arising from
95 large-scale extrapolations of heterogeneous wetlands have also been noted (Bridgman et al.,
96 2013).

97 One key challenge to upscaling is the high within-lake spatial variability of methane
98 emissions. Total fluxes measured from vegetated (Villa et al., 2021) and shallow (Natchimuthu
99 et al., 2016) zones can be statistically greater than those from open water and have been
100 attributed to the majority of whole-lake emissions (Saunois et al., 2020). Estimates derived from
101 deep lake centers have been shown to underestimate total flux by 5-78% in select lakes
102 (Natchimuthu et al., 2016). Plant-mediated fluxes can be significant at the landscape scale, for
103 example exceeding peatland emissions in southern Finland by 30%, despite covering only 40%
104 as much area (Bergström et al., 2007). Another study of three Finnish lakes found that the
105 vegetated littoral zone produced 66-77% of whole-lake emissions (Juutinen et al., 2003).
106 Combined globally, emergent macrophytes are estimated to emit 11% of the equivalent from all
107 open water lakes, rivers, and reservoirs (Bastviken et al., 2011). As the most “wetland-like” zone
108 within lakes, littoral zones are important sources of carbon and known methane emission hot
109 spots (Bergström et al., 2007; Burger et al., 2016; Huttunen et al., 2003; Juutinen et al., 2003;
110 Larmola et al., 2004), with exceptions (Jansen et al., 2020). However, littoral zone area is
111 difficult to quantify accurately because its extent is classified by light penetration into the water
112 column (Wetzel, 2001) and not by characteristics that are easily delineated by remote sensing.
113 Fortunately, the extent of emergent macrophytes growing in water $< \sim 1.5 \text{ m}$ deep in the upper
114 littoral zone are more easily detected. These plants can act as conduits to the atmosphere for
115 methane produced in lake sediments (Dacey and Klug, 1979; Colmer, 2003). They also produce
116 carbon compounds that are preferentially consumed by methanogens (methane-producing
117 bacteria), and their decomposing biomass and root exudates are a large contributor to sediment
118 organic carbon (Christensen et al., 2003; Joabsson, Christensen, & Wallén, 1999; Ström et al.,
119 2005). Previous studies have noted the tendency for small (Michmerhuizen, Striegl, &
120 McDonald, 1996; Bastviken et al., 2004; Holgerson & Raymond, 2016; Engram et al. 2020) and
121 shallow (West et al., 2015; Wik et al., 2016a; Li et al., 2020) lakes to emit more methane than
122 larger and deeper ones. DelSontro et al. (2018b) successfully modeled lake methane
123 concentration as a function of distance from the littoral zone, horizontal transport and oxidation,

124 and oxic epilimnetic production, which highlights the outsized importance of littoral methane
125 production. Notably, not all properties of littoral zones come from their vegetation. Their relative
126 shallowness is also a factor, as depth often prohibits methane ebullition due to water overburden
127 pressure (Bastviken et al., 2004, Langenegger et al., 2019), although there are exceptions
128 (Huttunen et al., 2003). Shallow waters may also contain distinct sediment organic matter
129 composition and less opportunity for microbe-mediated oxidation of dissolved methane
130 (DelSontro et al., 2016). Finally, diffusive fluxes measured in the littoral zone may be driven by
131 terrestrial inflows (Paytan et al., 2015, Natchimuthu et al., 2016), and offshore fluxes are
132 diminished by oxidation during transport (DelSontro et al., 2018b). Thus, methane emissions in
133 lakes are spatially variable, with highest emissions coming from littoral zones, particularly with
134 vegetation.

135 This challenge of accounting for spatial heterogeneity is exacerbated by lack of data in
136 the littoral or vegetated zones (DelSontro et al. 2018b; Desrosiers et al., 2022). The Boreal–
137 Arctic Wetland and Lake Methane Dataset (BAWLD-CH₄; Kuhn et al., 2021a; Kuhn et al.,
138 2021b) is the first synthesis study we are aware of that notes which part of the lake ebullition
139 fluxes were measured (center, edge, or whole lake). However, only 143 of the 553 records
140 actually contain within-lake location, and of these, only one was measured from an edge, with 19
141 from centers and 123 from whole-lakes. Among lake methane studies, plant-mediated emissions
142 are measured least frequently of all lake pathways (Bastviken et al., 2011; Wik et al., 2016a),
143 along with open-water emissions near plants, so methane upscaling estimates in lakes (DelSontro
144 et al., 2018a; Tranvik et al., 2009) usually rely solely on pelagic diffusion and ebullition
145 (DelSontro et al. 2018; Desrosiers et al., 2021), with biases introduced by insufficient within-
146 lake sampling sites (Wik et al., 2016b). For these reasons, lake methane measurements are under-
147 represented in vegetated and littoral zones, even among the few studies that report sampling
148 location.

149 Another key challenge to upscaling is that littoral and vegetation coverage in lakes are
150 poorly constrained. Duarte et al. (1986) suggested that emergent macrophytes colonize on
151 average 7% of a lake regardless of its area, while submerged macrophyte coverage generally
152 declines with area. They list light availability, sediment characteristics, and trophic status as key
153 characteristics for macrophyte growth, with slope as the greatest predictor of emergent
154 macrophyte coverage. Others have theorized that the percent of a lake's surface area covered
155 with macrophytes scales with nitrogen concentration and the inverse of mean depth (Smith and
156 Wallsten 1986), or scales inversely with lake area (Michmerhuizen et al., 1996) or perimeter
157 (Bergström et al., 2007). Mäkelä et al. (2004) similarly found that an average of 6% (range: 1-
158 100%) of total lake area was covered by macrophytes in a sample of 50 lakes and that total
159 fractional macrophyte coverage per lake steeply declined with lake area. Zhang et al. (2017)
160 compiled a synthesis database of aquatic macrophytes in 155 global lakes and observed an
161 average coverage of 26% (range: 0.000-100%) with an accelerating decline since 1900.

162 Remote sensing studies have used both optical and synthetic aperture radar (SAR)
163 sensors to map macrophytes in lakes. Optical satellites are better suited to detecting vegetation
164 type, while SAR can detect water even through vegetation canopies (Hess et al., 1990). Ghirardi
165 et al. (2019) used optical Sentinel-2 satellite data to map submerged aquatic macrophytes in an
166 Italian lake and noted both inter- and intra-annual variations in aerial coverage. Nelson et al.
167 (2006) used Landsat Thematic Mapper imagery to map various types of macrophytes in 13 lakes
168 in Michigan, USA and found total macrophyte coverage ranging from 5-42%. Ganju et al. (2017)

169 used air imagery and elevation data to derive the unvegetated/vegetated marsh ratio (UVVR) for
170 tidal marshes, which scales with sediment budget and has typical values < 0.4 . Zhang et al.
171 (2018) used TerraSAR-X SAR imagery to map macrophytes in nine Brazilian reservoirs and
172 similarly found large spatial and temporal variation in coverage. Thus, many remote sensing
173 studies have demonstrated spatial and/or temporal differences in aquatic macrophyte cover, yet
174 few have measured total coverage across large geographical areas and numerous lakes. Lake
175 macrophyte area statistics, therefore, remain confined to a handful of studies of small numbers of
176 lakes.

177 Here, we aim to quantify the fractional coverage of emergent vegetation for 4,572 lakes
178 across four Arctic-boreal regions in order to assess their potential importance in scaling methane
179 emissions. To estimate coverage, we use the canopy-penetrating properties of L-band synthetic
180 aperture radar (SAR) flown during the NASA Arctic-Boreal Vulnerability Experiment (ABoVE)
181 airborne campaign (2017-2019). Although floating-leafed macrophytes are relevant to the
182 methane budget, they cannot be reliably detected with this technique due to similar surface
183 roughness with water waves and thus are omitted here. Next, we compile paired measurements
184 of methane flux (new data and literature) via all pathways from open water and emergent
185 macrophyte regions of lakes. Finally, we use these flux measurements and our remote sensing-
186 derived ranges in emergent vegetation coverage to estimate its impact on lake methane
187 emissions. We conclude with discussion of the causes of regional differences, some broader
188 recommendations for landscape-scale methane upscaling, study limitations, and
189 recommendations for future research.

190 **2 Study areas, data sources, and methods**

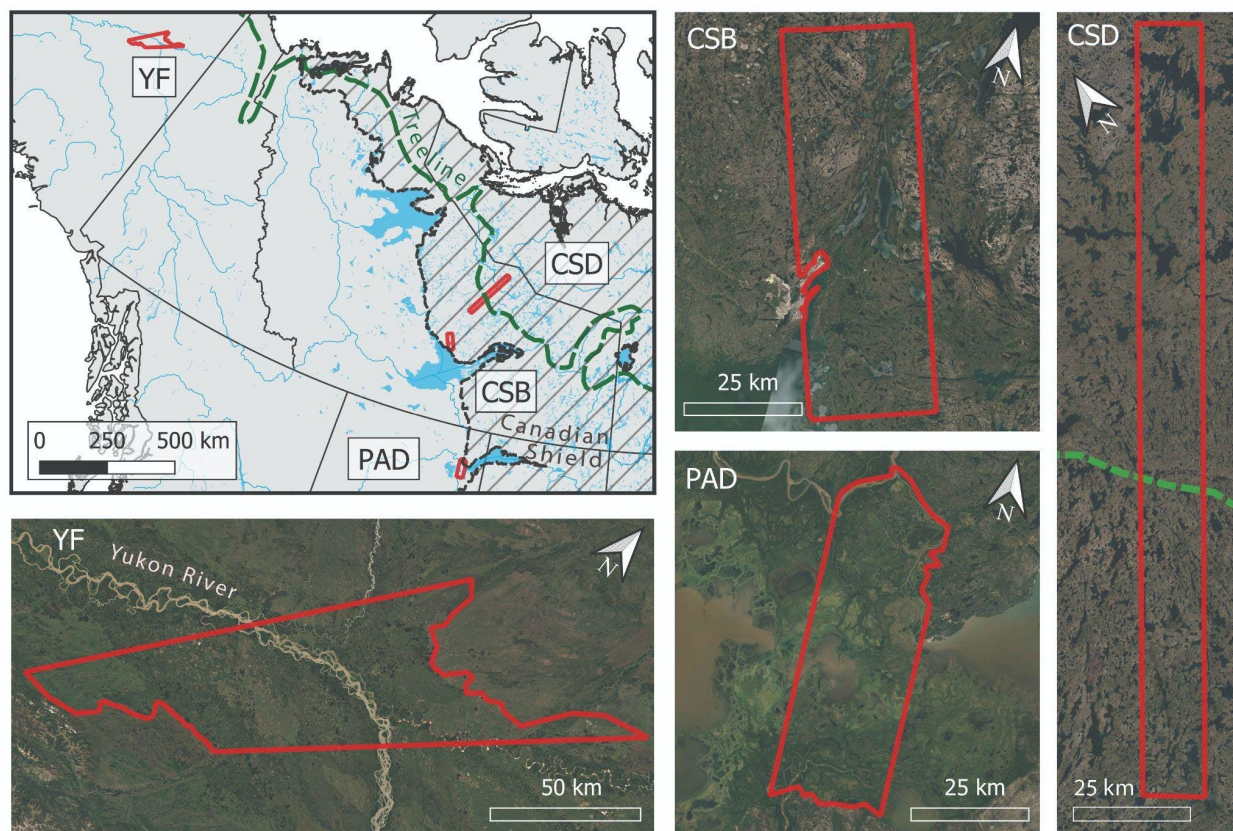
191 2.1 Study areas

192 The NASA Arctic-Boreal Vulnerability Experiment (ABoVE) campaign is a decade-long
193 effort to measure environmental change in the Arctic and boreal regions of western North
194 America via coordinated ground measurements and airborne remote sensing (Miller et al., 2019).
195 Here, we focus on four study areas within the ABoVE domain, each corresponding to one or
196 more flight lines from its airborne campaigns:

- 197 1) Peace-Athabasca Delta, Alberta, Canada (PAD);
- 198 2) Southern Canadian Shield near Baker Creek (CSB), Northwest Territories, Canada;
- 199 3) Interior Canadian Shield near Daring Lake (CSD), Northwest Territories, Canada; and
- 200 4) Yukon Flats National Wildlife Refuge, Alaska, USA (YF).

201 These four study areas were chosen because of their high lake density and contrasting geological,
202 hydrological, and ecological conditions. The PAD is one of the world's largest inland deltas and
203 is located on the western edge of Lake Athabasca (**Figure 1**). The overall relief of its lowland
204 regions is 11 m, causing numerous marsh-type wetlands, mudflats, and lakes, many of which are
205 recharged by the Athabasca River (Pavelsky & Smith, 2008), and more rarely, by ice-jam floods
206 in the Peace River (Timoney, 2013). These floods can inundate up to 80% of the 5,600 km² delta
207 (Töyrä & Pietroniro, 2005; Wolfe et al., 2006), while in typical years, 26% is covered by
208 intermittently-inundated wetlands (Ward & Gorelick 2018). It is a Ramsar Wetland, UNESCO
209 World Heritage site, and home to numerous endemic species of birds, fish, and mammals
210 including the endangered whooping crane and the largest remaining herd of wood bison (Parks

211 Canada, 2019). The two Northwest Territories study areas (CSD, CSB) are located on the
 212 Canadian Shield, the world's largest deposit of Precambrian-age bedrock and source of the oldest
 213 known terrestrial rocks (Slaymaker, 2016). Deglaciated only nine thousand years ago and with a
 214 rocky, sparse surface drainage pattern, the Shield is also the world's most lake-rich region and
 215 contains many peatlands (Slaymaker, 2016; Spence & Woo, 2006). CSB is underlain by
 216 discontinuous permafrost, while CSD crosses the tree line and contains a transition to continuous
 217 permafrost and the tundra/taiga ecotone (**Figure 1**). The YF is underlain by discontinuous
 218 permafrost in alluvial soils and contains lakes of various hydrologic connectivity to the Yukon
 219 River and its tributaries (Anderson et al. 2013, Johnston et al., 2020). Like the PAD, the YF has
 220 flat topography, permitting seasonal flooding during the early summer to cover large areas, and it
 221 is a source of both lateral riverine and water-air carbon fluxes (Striegl, et al., 2012). All four
 222 study areas are home to multiple indigenous and First Nation communities, as well as the city of
 223 Yellowknife (CSB) and numerous smaller settlements.



225 **Figure 1.** Location map of study areas (YF = Yukon Flats; CSD = Canadian Shield, Daring
 226 Lake; CSB = Canadian Shield, Baker Creek; PAD = Peace-Athabasca Delta). Study area
 227 boundaries (red polygons) are derived from intersecting UAVSAR airborne flight coverage with
 228 physiographic boundaries. Major water bodies are shown in blue; Canadian Shield with
 229 stippling, and the northern tree line limit (Brown et al., 2002) in green.

230

231 2.2 Data sources

232 2.2.1 Airborne polarimetric SAR

233 L-band synthetic aperture radar (SAR) data from the Uninhabited Aerial Vehicle
 234 Synthetic Aperture Radar (UAVSAR) were obtained in multi-look ground-projected format
 235 (GRD) and reprojected to ~5.5 m spatial resolution (NASA/JPL 2017-2019) on the ABoVE
 236 Science Cloud computing environment. With a wavelength of 23.8 cm, UAVSAR has been used
 237 extensively for vegetation mapping and inundation detection, including in lowlands or deltas
 238 with flooded vegetation (Ayoub et al., 2018; Jensen et al., 2021; Z. Zhang et al., 2017). All
 239 available ABoVE UAVSAR flight dates from non-contiguous days during summers 2017-2019
 240 were used. Both early (June) and late (August-September) summer images were acquired by
 241 UAVSAR in 2017, and only late summer/early autumn dates were imaged in 2018 and 2019.

242

243 2.2.2 Water and land cover maps

244 Several ABoVE land cover data sets were referenced to help build a land cover training dataset
 245 for UAVSAR (see **Section 2.3.1**). High-resolution imagery and derivative water masks were
 246 obtained from the AirSWOT color-infrared camera (Kyzivat et al. 2018; Kyzivat et al. 2019;
 247 Kyzivat, et al. 2020), supplemented by high-resolution satellite imagery from Maxar
 248 (<https://evwhs.digitalglobe.com/myDigitalGlobe/>). Two satellite-based land cover maps
 249 available for the ABoVE domain were also referenced (Bourgeau-Chavez et al., 2017, 2019;
 250 Wang et al., 2019; Wang et al., 2019). Although these maps use a different classification scheme
 251 than our derived UAVSAR classification, they are particularly useful for partitioning between
 252 trees, shrubs, and graminoid vegetation.

253

254 2.3 Methods

255 2.3.1 Land cover classification training dataset

256 To estimate lake emergent macrophyte coverage (A_{EV}), a land cover training dataset was
 257 created using inundation status from field measurements in 2015 and 2017-2019 and vegetation
 258 categories from ABoVE land cover maps (Bourgeau-Chavez et al., 2017, 2019; Wang et al.,
 259 2019; Wang et al., 2019). As part of the field measurements, lake and wetland shorelines and
 260 vegetation zones were mapped by field teams carrying handheld GPS receivers, as described in
 261 Kyzivat et al. (2019). In YF, airborne GPS tracks from a low-hovering helicopter were used, as
 262 no suitable ground GPS tracks were available. Contextual photos were also taken by camera,
 263 both from the ground and from aircraft windows, and by uninhabited airborne vehicles (UAVs).
 264 UAV photos were processed into orthomosaics using DroneDeploy web software. All of these
 265 measurements were digitized into polygon shapefiles in ArcGIS 10.6 denoting 13 land cover
 266 classes falling into five broad categories of open water, dry land and three types of emergent
 267 vegetation (**Table 1**). The resulting vector data set was used to train and validate a supervised
 268 classification from the radar data (Kyzivat et al., 2021a).

269

Broad Grouping	UAVSAR land cover class
----------------	-------------------------

Open surface water	Open Water (OW), Rough Water (RW), Sedimentary Bar (SB), Wet Herbaceous (WH)
Wet Graminoid	Wet Graminoid (WG)
Wet Shrub	Wet Shrub (WS)
Wet Forest	Wet Forest (WF)
Dry land	Dry Graminoid (DG), Dry Shrub (DS), Dry Forest (DF), Bank Scarp Double-Bounce (BS), Dry Woodland (DW), Bare Ground (BG)

270 **Table 1.** Classification Schema: RW refers to wind roughening at the time of acquisition. WG
 271 refers to cattails (*Typha latifolia*), bulrushes (*Scirpus* spp.), and sedges (*Carex* spp.), as well as
 272 aquatic horsetails (*Equisetum fluviatile*). WS typically refers to willows (*Salix* spp.). DW refers
 273 to a mix of trees and shrubs as defined by Wang (2019). WH refers to water lilies (*Nuphar*
 274 *variegatum*), and both WH and SB were not separable from the other open water classes. Further
 275 details are in the accompanying data publication (Kyzivat et al., 2021a).

276

277 2.3.2 Synthetic aperture radar data pre-processing

278 UAVSAR GRD data for the PAD, YF and CSB flight lines were transformed to the C3
 279 complex covariance matrix using PolSAR Pro 6.0 software. Images were corrected for incidence
 280 angle-dependent backscatter using a fitted exponential function multiplied by the cosine of
 281 incidence angle as per Ulander (1996) and Zhang et al. (2017). Due to its more rugged
 282 topography, CSD was corrected for both incidence angle and terrain slope as per the look-up
 283 table method of Simard et al. (2016). For all flight lines, a Freeman-Durden polarimetric
 284 decomposition was performed. The decomposition comprises a physical scattering model and is
 285 commonly used to identify scattering mechanism contributions to each pixel (single bounce,
 286 modeled as Bragg scattering; double bounce, modeled as from a pair of orthogonal surfaces; and
 287 volume scattering, modeled as from a cloud of randomly-oriented dipoles) (Freeman & Durden,
 288 1998). Although it is known to overestimate the double bounce component (Chen et al., 2014), it
 289 is sufficient as an input feature to an empirical, machine-learning based classification.

290 2.3.3 Land cover classification

291 Each of the three scattering mechanism output bands was used for feature extraction via
 292 three moving-window filters designed to introduce spatial contextual information for the
 293 classifier. The chosen filters were standard deviations, offsets oriented along the radar look
 294 direction, and an edge-preserving guided filter to reduce speckle (**Table S.2**). Additional input
 295 bands of incidence angle and elevation-derived indexes were tested, but ultimately omitted, due
 296 to their high spatial autocorrelation, which led to model over-fitting. The training class BS was
 297 developed specifically to identify bright double bounce scattering between water surfaces and
 298 steep bank scarps, which would otherwise have appeared as inundated vegetation. SB and WH
 299 (defined as protruding <20 cm from the water surface, as determined from field measurements)
 300 were found to be inseparable from OW, so they were treated as open surface water in the
 301 analysis. The radar dataset was further prepared for classifier training by randomly under-
 302 sampling the majority training classes and cropping out pixels taken at low incidence angles.

303 Incidence angle limits as well as filter parameters (**Table S.2**) were chosen by trial and error.
304 Finally, pixel values within training polygons in all input bands from the appropriate date were
305 extracted, and the results split using stratified sampling into training (85%) and validation (15%)
306 datasets with 15 bands each. A description of this workflow, parameter settings, and other
307 technical details is provided in **Table S.2**.

308 Finally, a random forests classifier was trained using the TreeBagger function in Matlab
309 R2017b and evaluated using the validation dataset via the confusion matrix and Cohen's kappa
310 coefficient. One model was used for the areas with incidence angle correction and another for the
311 CSD area with the look-up table correction. The models were then applied over the extent of
312 their corresponding study areas for all available dates. The original 13 classes were aggregated
313 into the five generalized classes for analysis (**Table 1**).

314

315 2.3.4 Quality control and conversion to emergent vegetation coverage

316 The derived five-class land cover maps were used to identify emergent macrophyte and
317 open water areas and quantify their total landscape coverage. First, maps were clipped to the
318 intersection of all flight lines per study area excluding any roads or urban areas, if present. Raster
319 mosaics were created for the PAD and YF, since they were acquired in multiple flight lines on
320 most dates (**Table S.1**). Next, candidate lakes were identified as connected pixel groups of at
321 least five pixels with at least one open water pixel and any number of inundated vegetation pixels
322 (or none at all). This criterion permitted inclusion of open water wetlands, since there is no
323 reliable way to differentiate them from lakes and ponds. Rivers were removed by applying a
324 manually-created river mask, modified from Kyzivat et al. (2019). Lake emergent vegetation
325 (*ALEV*) were operationally defined as emergent vegetation classes 8-connected to lakes, with the
326 remaining emergent vegetation pixels considered wetlands (*AWEV*). Although dependent on pixel
327 size, this definition permitted a consistent definition across all study areas. At this stage, the total
328 landscape coverage of *ALEV* (wet graminoid, shrub, and forest classes) and open water were
329 calculated so they could be compared between dates.

330 Although there is scarce data for methane emission from trees and shrubs along lake
331 shores, we included them in the sensitivity analysis because: 1) 69% of *ALEV* is comprised of
332 graminoid vegetation and this value increases to >97% after correcting for double counting (see
333 **3.1.1**); 2) There is no mixed coverage class, meaning there is likely still graminoid vegetation
334 present, but hard to detect; 3) Data scarcity makes it hard to account for them separately; and 4)
335 Many of the factors that make vegetated water surfaces high emitters are shared between
336 vegetation types, such as shallowness, proximity to terrestrial inputs, variable inundation, and
337 presence of root systems. In fact, these dynamically-inundated water surfaces with woody
338 vegetation, which could also be called littoral swamps, have been shown to emit methane four
339 orders of magnitude greater than temperate forest soil uptake (Hondula et al., 2021). This
340 observation underscores the importance of accounting for regions of emergent lake vegetation
341 separately from open water, while being sure to exclude any regions otherwise accounted for as
342 wetlands (see **2.3.7**).

343 To calculate *ALEV* coverage on a per-lake basis, water bodies smaller than 250 m²
344 (0.00025 km² or 7-8 px) were discarded, since they were too small to consistently resolve and
345 likely included false detections. Although hardly affecting total lake area, false detections of

346 lakes would be disproportionately small and thus impact the distribution of A_{LEV} . Partially
347 observed lakes intersecting the flight line boundary were discarded as well, since A_{LEV} could not
348 be reliably measured. A third category of lakes were discarded if they did not overlap with any
349 water pixels in the 2017 AirSWOT color-infrared camera open water masks, which had a slightly
350 narrower ground footprint in all study areas. By comparing our UAVSAR retrievals to an
351 independent, optical data set, this step removed many falsely-identified lakes caused by
352 classification error. Finally, we calculated the areas of the remaining lakes and the fractional area
353 of their emergent vegetation (A_{LEV}) coverages, defined as the proportion of pixels in a lake
354 classified as any of the three inundated vegetation classes. For visualization and analysis, these
355 data were divided into 24 logarithmically-spaced lake area bins across the four study areas, and
356 the mean, lake area-weighted mean, and median A_{LEV} computed for each study area. For each
357 study area, confidence intervals were calculated for each of the 24 bins and for the area-weighted
358 means using the 95th percentile of 10,000 bootstrapped simulated datasets.

359

360 2.3.5 Adjusting estimate to avoid double-counting wetlands

361 Our method for detecting emergent vegetation excludes wetlands based on lack of pixel
362 connectivity to open water. Although this method conserves total area and thus does not double-
363 count any pixel to more than one land cover class, this partitioning includes open-water and
364 littoral wetlands as parts of lakes. As a result, our estimate of A_{LEV} would be too high because it
365 treats areas typically considered to be wetlands (e.g. in methane models) as parts of lakes, which
366 is precisely the double-counting between datasets described by Thornton et al. (2016). To correct
367 for this over-estimate of total lake area, we obtained two leading global lake datasets,
368 GLOWABO (Verpoorter et al., 2014) and HydroLAKES (Messenger et al., 2016) and compared
369 total lake extent between the datasets and our own. First, since the global datasets were made at a
370 coarser geographic scale, USAVSAR lakes below the appropriate minimum size threshold were
371 excluded (0.002 km² for GLOWABO and 0.1 km² for HydroLAKES). Even so, there were still
372 many more lakes detected by UAVSAR (and some only detected by one of the other datasets), so
373 spatial selection in the python package geopandas 0.10.2 (Jordahl et al., 2021) was used to
374 exclude any lakes in either dataset that didn't overlap at least partly with a lake in the dataset to
375 which it was being compared. This exclusion ensured that we were only comparing areas within
376 commonly-detected lakes and not simply assessing lake mapping accuracy between the datasets,
377 which have vastly different scales and time domains. Next, both datasets were rasterized to the
378 UAVSAR pixel grid for the corresponding scene, typically 5.5 by 5.5 m pixels. Then, for each
379 study area, a confusion matrix was computed between the UAVSAR dataset and each of the
380 others for all pixels not denoted as land in both candidate datasets. These matrices were used to
381 compute the scalar c , which is used in **Equation [1]** and denotes how much of UAVSAR A_{LEV}
382 falls within global dataset lakes, with the remainder assumed to already be mapped as wetlands
383 with adequate accounting of methane emissions.

384 The calculation ignores the effects of changing inundation during the 10-20 years
385 between data acquisitions, as well as errors arising from the global datasets having less-precise
386 georeferencing. It is also limited to only the large lakes that could be compared between datasets.
387 Since these biases would also exist in any modeling study using GLOWABO or HydroLAKES,
388 we have made no attempt to correct for them, which would also be beyond the scope of this
389 work.

390 2.3.6 Methane flux chamber measurements

391 24 methane fluxes were measured at 15 lakes in the PAD during July and August 2019
392 (Kyzivat et al. 2021, **Figure S.6**). The sampling schedule permitted no more than one or two
393 visiting days per lake, so the measurements represent a broad, geographic sampling within the
394 PAD at the expense of frequent measurements in any one lake. This sampling approach allowed
395 for better, but still limited extrapolation to the 470 UAVSAR-observed lakes in the PAD. In all
396 15 lakes, single 15-minute fluxes were taken from an open water region near the lake center via
397 inflatable raft, anchored canoe, or motorboat. In five lakes, one to three additional flux
398 measurements were made amidst emergent macrophytes of different species (corresponding to
399 the wet graminoid land cover class) short enough to fit into the flux chamber without excessive
400 disturbance. The chamber comprised an inverted 25.4 cm tall, opaque white bucket with a 34.2
401 cm diameter opening wrapped with a buoyant skirt made of foam tubing. An infrared greenhouse
402 gas analyzer (EGM-4, PP Systems) was used to measure chamber air carbon dioxide (CO₂)
403 concentration and circulate chamber air via an inlet on the side of the chamber and an outlet in
404 the center of its ceiling. A metal handle was used to steady the bucket for a 15-minute
405 measurement period. At 0, 5, 10, and 15 minutes, gas samples were drawn from the chamber's
406 headspace through the gas analyzer inlet tubing and injected into evacuated exetainers using a 30
407 mL polypropylene syringe fitted with a 3-way stopcock for subsequent analyses of methane
408 concentration.

409 The samples were analyzed on a Shimadzu GC-2014 gas chromatograph for methane
410 partial pressure within two months of collection. Gas flux across the water-air interface was
411 calculated from the rate of change in the chamber methane concentration over the deployment
412 time and chamber area ($\text{mol}\cdot\text{min}^{-1}\cdot\text{m}^{-2}$). The rates of change of methane concentrations in the
413 chamber were generally linear with r^2 values greater than 0.90. Given this linear response,
414 ebullition was deemed negligible during the measurement periods. Thus, the closed, static
415 chamber measurements included both diffusive fluxes from the water surface as well as any
416 plant-mediated fluxes. For the three lakes where multiple emergent macrophyte fluxes were
417 taken at one location, measurements from each water zone were averaged by lake. Finally, for
418 sites where paired open water vs. littoral zone measurements were collected, we calculated the
419 vegetated: open water flux ratio (hereafter: flux ratio) as the ratio between the average emergent
420 macrophyte and open water measurements for each lake, where open water could include
421 submerged macrophytes not detectable with UAVSAR.

422 During sampling, care was taken not to disturb the sediment, and if any bubbles were
423 observed before or during the period, the measurement was aborted. Even so, three
424 measurements were extremely high, implying sediment disturbance. To avoid potential bias,
425 these measurements, which were greater than 2.2 standard deviations from the median, were
426 discarded (the next-highest value was 0.17 standard deviations from the median). These three
427 measurements all came from vegetated sites, so this data omission lessened the impact of
428 emergent vegetation in our subsequent analyses.

429

430 2.3.7 Published flux chamber measurements

431 In addition to our own field measurements, we compiled a synthesis dataset of 56 paired
432 flux measurements, with the aim of determining the flux ratio for each lake. 52 of these

433 measurements corresponded to vegetated versus open water fluxes, and were used for subsequent
434 calculations, while the remaining four were taken from shallow (typically with a 2 m cutoff)
435 versus deep regions of the lake, with no mention of adjacent macrophytes. Each lake pair
436 corresponded to one of 41 distinct lakes or lake regions during a single or multi-year-averaged
437 sampling season, published in 20 papers (Kankaala et al. 2005; 2013; Smith and Lewis 1992;
438 Larmola et al. 2004; Huttunen et al. 2003; Juutinen et al. 2003; Villa et al. 2021; Burger et al.
439 2016; DelSontro et al. 2016; Bergström et al. 2007; Striegl and Michmerhuizen 1998; Ribaudou et
440 al. 2012; Casper et al. 2000; Dove et al. 1999; Elder et al., 2022; Rey-Sanchez et al., 2018;
441 Desrosiers et al., 2021; Engram et al. 2020; Natchimuthu et al., 2016; Wik et al., 2013, **Table**
442 **S.3**). Lakes included boreal, tropical and temperate regions and were located in Finland, Quebec,
443 Ontario, Alaska, Colorado, Ohio, Minnesota, Italy, the UK, and the Amazon and Orinoco river
444 basins. For each paper, the average—whether seasonal or annual—vegetated and open water
445 measurements were recorded and converted, if necessary, to units of $\text{mg CH}_4/\text{m}^2/\text{day}$. Four
446 papers (Burger et al., 2016; Casper et al., 2000; Dove et al., 1999; Desrosiers et al., 2021)
447 separately measured each of the three methane emission pathways, and most of the others
448 focused on diffusion and/or plant-mediated fluxes. An additional five (Huttunen et al., 2003;
449 Juutinen et al., 2003; Larmola et al., 2004; Striegl and Michmerhuizen, 1998; Villa et al., 2021)
450 measured diffusion and ebullition in both lake zones, but did not place the flux chamber over
451 plants, thus not accounting for that pathway. One study (Bergström et al., 2007) did not provide
452 open water values, which we estimated based on lake area via the relationship of Holgerson and
453 Raymond (2016).

454 The vegetated: open water flux ratio R was calculated for each applicable lake (including
455 our field lakes) and divided by a correction factor of 1.33 to account for most measurements
456 being made either during ice-covered or ice-free seasons, but not during ice melt, when open-
457 water emissions can temporarily spike. The correction factor, averaged from Wik et al. (2016a)
458 and Denfeld et al. (2018), comes from statements that 23% and 27% of emissions of ice-covered
459 lakes, respectively, are attributed to ice-melt fluxes. Although the lake upscaling calculation by
460 Rosentreter et al. (2021) also uses a spatiotemporal ice-cover correction with the opposite effect
461 of the ice-melt pulse correction, we have omitted it here, assuming it affects both vegetated and
462 unvegetated areas equally. The adjusted flux ratio R' therefore comes from measurements of
463 three methane flux pathways, collected from both littoral vegetation and shallow open water in
464 all seasons, and reflects adjustments to account for unmeasured ice-melt pulses.

465 Many papers stated the area covered by emergent macrophytes, but if not, Google Earth
466 Pro and QGIS 3.10.11 were used to digitize, map project, and measure the approximate coverage
467 area, with attention paid to the papers' description of the vegetation for context. Coverage areas
468 were assigned an uncertainty value (typically 2–5%) based on interpretation of the methods used
469 or confidence in our digitizing result. Although challenging to compare across methodologies,
470 geographic regions, and plant types, this dataset served as a best estimate of flux ratios from a
471 diverse global sample of lakes.

472

473 2.3.8 Sensitivity analysis

474 Likely ranges in whole-lake methane emissions were calculated using the following
475 equation, mapped lake areas, and the compiled flux dataset:

$$F_{total} = c * A_{LEV} * R' * f_{OW} + (1 - c * A_{LEV}) * f_{OW} \quad [1]$$

where c is a scalar ≤ 1 , described in section 2.3.7, that corrects for potential double-counting of UAVSAR-observed emergent vegetation as wetlands contained in modeling datasets; F_{total} is the calculated total lake flux (mg CH₄/day); A_{LEV} is the mean fractional emergent vegetation area per lake (unitless); f_{OW} is the flux per unit area of open water (mg CH₄/m²/day) and R' is the corrected ratio between area-weighted emergent macrophyte and open water fluxes (unitless). The impact of vegetation on whole-lake flux was calculated as:

$$I = \frac{F_{total} - f_{OW} * 1}{f_{OW} * 1} \quad [2]$$

where I is unitless and represents the percent increase from differentiating between open water and emergent vegetation within lakes. All calculations are performed over unit areas (normalized to percentages of the total mapped lake area) to highlight that the calculation is independent of domain size. I is sensitive only to the flux ratio R and independent of the individual magnitudes of open or vegetated water fluxes. As such, flux variables F and f are distinct; although working with normalized areas causes them to have the same units, f refers to fluxes from a particular lake surface, while F is an area-weighted average of fluxes from these surfaces. The ones are retained to indicate division by 100% of the lake area.

For broader context, we also re-normalized I to compare the difference in emissions to total inland aquatic fluxes, rather than only to lakes:

$$I' = I * \frac{F_l}{F_{aq}} \quad [3]$$

where I' is again unitless and represents the percent increase on aquatic fluxes (lakes/ponds, reservoirs, rivers, wetlands) in our study domain resulting from accounting for lake emergent vegetation; F_l is a total lake flux and F_{aq} a total aquatic flux (in Tg CH₄/yr) computed by process-based modeling. We set $F_{aq} = 261$ and $F_l = 55.8$ Tg CH₄/yr, using total bottom-up aquatic flux values from Rosentreter et al. (2021).

Equations [1] – [3] were applied using the median values of R and f_{OW} and the lake area-weighted mean A_{LEV} . Median values were used due to the skewed distributions of R and f_{OW} . The equations were also applied to the bootstrapped confidence intervals of A_{LEV} in order to estimate uncertainty.

504

505 3 Results

506 3.1 Inundation patterns at the landscape scale

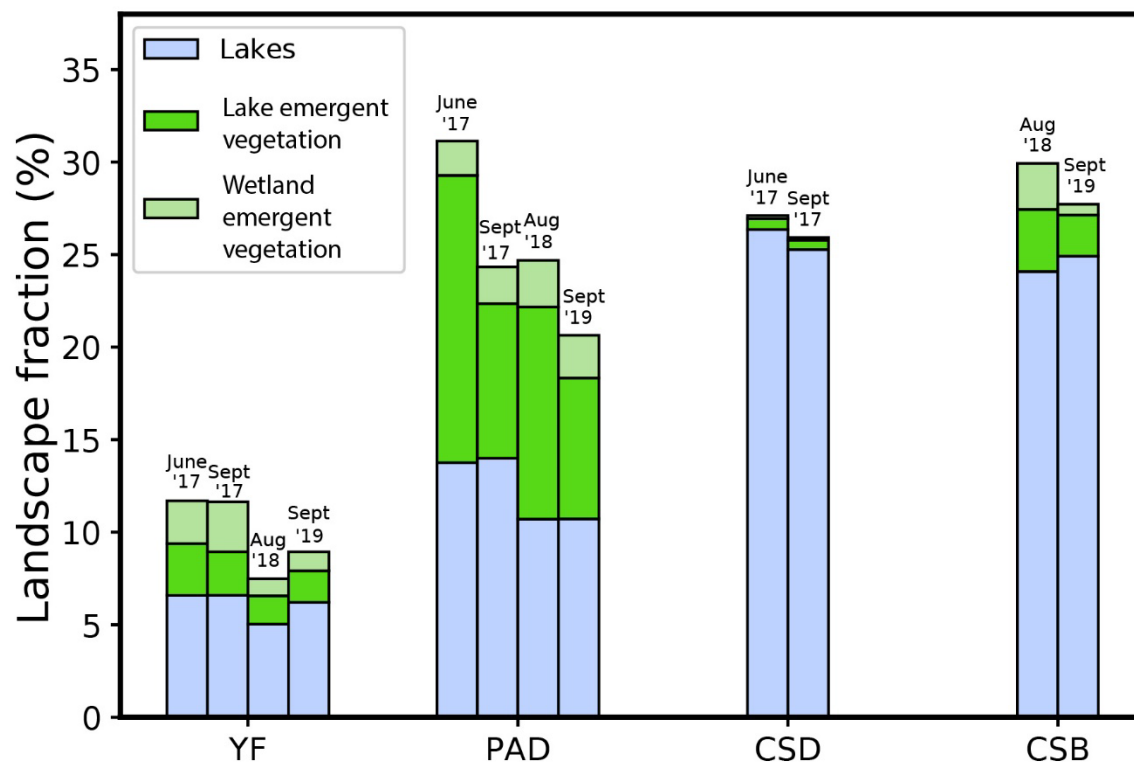
507 3.1.1 Regional and seasonal inundation characteristics

508 Significant open water, emergent vegetation, and wetland fractional areas are found in all
 509 study areas, vary seasonally as well as regionally, and are particularly extensive in the PAD and
 510 YF. The total area of the landscape covered by lake emergent vegetation (LEV) varies from 0.5 –
 511 0.6 % (CSD), 2.2 – 3.4 % (CSB), 7.6 – 15.5 % (PAD), and 1.7 – 2.8 % (YF) over the 2017-2019
 512 observational period (**Figure 2, Table 2**). In comparison, wetland emergent vegetation (A_{WEV})
 513 covers $\leq 2.7\%$ of the area in all sites (mean of 1.4%, **Table 2**). Most of the emergent vegetation
 514 is classified as either wet graminoid (WG, weighted mean of 69%) or shrub vegetation (WS,

515 29%), with wet forest comprising <1% of this area for all areas except YF, for which it covers a
 516 mean of 5.9%. When only considering LEV that falls within a global dataset lake (the double-
 517 counting correction), the graminoid fraction increases to 99.1% (GLOWABO) or 98.7%
 518 (HydroLakes), which provides further confidence that the remaining LEV is indeed littoral
 519 vegetation and not an adjacent, forested wetland, at least for large lakes in the global datasets.
 520 Virtually all detected emergent vegetation lies adjacent to shorelines, with < 0.2% of their area
 521 occurring completely within a lake with no connectivity to non-island land. These patterns show
 522 that the dominant littoral vegetation type in the study areas is graminoids, which almost always
 523 occur at the interface between land and water.

524 In all applicable study areas, total inundation (open water plus emergent vegetation) is
 525 greater or equal in the early summer (June) than in late summer (August/September), likely due
 526 to snowmelt. In the PAD, this change is caused by decreased LEV, with emergent wetland
 527 vegetation remaining constant, implying that seasonal inundation changes occurred in flood-
 528 tolerant eulittoral vegetation (**Figure 2, Table 2**). Thus, regional variations in emergent
 529 vegetation, as well as open water, are greater than seasonal/interannual variations within study
 530 areas.

531



533 **Figure 2.** Significant lake emergent vegetation (LEV) is found in all study areas, varies
 534 seasonally as well as regionally, and is particularly extensive in the lowland PAD and YF. This
 535 chart shows landscape fractional areas of open water and LEV classes for the Yukon Flats (YF),
 536 Peace-Athabasca Delta (PAD), Canadian Shield – Daring Lake (CSD), and Canadian Shield –
 537 Baker Creek (CSB), derived from airborne UAVSAR. LEV is defined as emergent vegetation

538 adjacent to open water, with remaining areas assigned to wetlands (WEV). Month and year of
 539 UAVSAR flight acquisitions appear in text above each column.

	Study area	Extent (km ²)	Lake count	Lake fraction (%)					Landscape area (km ² , %)						
				A _{LEV}	A _{WF}	A _{VIS}	A _{WIG}	A _{LEV} (median)	A _{LEV} (unweighted)	Lake open water	LEEV	WF	WS	WG	WEV
CSD	June 2017	3037	4918	1.1 [0.9, 1.4]	0.0 [0.0, 0.0]	0.0 [0.0, 0.1]	1.1 [0.9, 1.3]	0.0%	2.0%	800 [25.4%]	18 [0.6%]	0 [0.0%]	1 [0.0%]	17 [0.6%]	3 [0.1%]
CSD	Sept 2017	3037	4975	0.9 [0.6, 1.1]	0.0 [0.0, 0.0]	0.0 [0.0, 0.0]	0.8 [0.6, 1.1]	0.0%	3.8%	767 [25.3%]	16 [0.5%]	0 [0.0%]	0 [0.0%]	15 [0.5%]	2 [0.1%]
CSD		3037	4947	1.0 [0.8, 1.2]	0.0 [0.0, 0.0]	0.0 [0.0, 0.1]	1.0 [0.7, 1.2]	0.0%	2.9%	784 [25.9%]	17 [0.5%]	0 [0.0%]	1 [0.0%]	16 [0.5%]	3 [0.1%]
CSB	Aug 2018	1155	376	8.6 [5.8, 14.1]	0.0 [0.0, 0.1]	2.3 [1.7, 3.6]	6.2 [4.1, 10.5]	20.4%	26.6%	278 [24.1%]	39 [3.4%]	0 [0.0%]	11 [1.0%]	28 [2.4%]	29 [2.5%]
CSB	Sept 2019	1160	378	5.5 [3.6, 9.0]	0.0 [0.0, 0.1]	0.7 [0.5, 1.1]	4.7 [3.1, 7.9]	11.3%	17.5%	289 [24.9%]	26 [2.2%]	0 [0.0%]	4 [0.3%]	22 [1.9%]	7 [0.6%]
CSB		1158	377	7.0 [4.7, 11.5]	0.0 [0.0, 0.1]	1.5 [1.1, 2.3]	5.5 [3.6, 9.2]	15.9%	22.1%	284 [24.5%]	32 [2.8%]	0 [0.0%]	7 [0.6%]	25 [2.1%]	18 [1.5%]
PAD	June 2017	1339	347	65.5 [56.5, 75.3]	0.7 [0.2, 1.3]	35.3 [28.2, 42.6]	29.5 [21.4, 38.8]	63.5%	58.3%	184 [13.8%]	208 [15.5%]	2 [0.1%]	73 [5.4%]	133 [10.0%]	25 [1.8%]
PAD	Sept 2017	1338	729	52.1 [42.8, 61.6]	0.1 [0.0, 0.3]	13.8 [9.0, 19.5]	38.2 [31.4, 45.3]	60.5%	56.2%	187 [14.0%]	112 [8.4%]	0 [0.0%]	18 [1.3%]	94 [7.0%]	26 [1.9%]
PAD	Aug 2018	1338	366	61.4 [51.8, 70.8]	1.1 [0.3, 1.9]	39.3 [31.1, 47.6]	21.1 [15.8, 27.7]	68.4%	62.0%	143 [10.7%]	153 [11.4%]	1 [0.1%]	64 [4.8%]	88 [6.6%]	34 [2.5%]
PAD	Sept 2019	1336	437	56.6 [49.2, 65.2]	0.3 [0.0, 0.6]	33.3 [26.9, 40.2]	22.9 [16.8, 31.1]	57.1%	57.7%	143 [10.7%]	102 [7.6%]	0 [0.0%]	42 [3.1%]	60 [4.5%]	31 [2.3%]
PAD		1338	470	58.9 [50.1, 68.2]	0.6 [0.1, 1.0]	30.4 [23.8, 37.5]	27.9 [21.3, 35.7]	62.4%	58.6%	164 [12.3%]	144 [10.7%]	1 [0.1%]	49 [3.7%]	94 [7.0%]	29 [2.1%]
YF	June 2017	2739	2687	24.9 [22.8, 27.2]	1.2 [0.2, 2.5]	4.0 [3.4, 4.8]	19.7 [18.0, 21.6]	31.8%	36.8%	180 [6.6%]	77 [2.8%]	4 [0.1%]	14 [0.5%]	58 [2.1%]	63 [2.3%]
YF	Sept 2017	2739	2857	22.6 [20.7, 24.7]	1.3 [0.3, 2.6]	5.5 [4.3, 6.8]	15.8 [14.6, 17.3]	27.0%	33.5%	180 [6.6%]	64 [2.3%]	4 [0.1%]	15 [0.6%]	45 [1.6%]	74 [2.7%]
YF	Aug 2018	2739	1784	22.4 [19.7, 25.3]	1.8 [0.3, 3.8]	4.6 [3.6, 6.0]	16.0 [14.3, 17.9]	17.0%	28.2%	138 [5.0%]	42 [1.5%]	3 [0.1%]	10 [0.4%]	30 [1.1%]	25 [0.9%]
YF	Sept 2019	2739	4533	18.5 [16.1, 21.2]	1.9 [0.4, 4.0]	2.3 [1.8, 3.0]	14.3 [12.7, 16.1]	15.6%	25.5%	170 [6.2%]	47 [1.7%]	3 [0.1%]	9 [0.3%]	35 [1.3%]	28 [1.0%]
YF		2739	2215	22.1 [19.8, 24.6]	1.5 [0.3, 3.2]	4.1 [3.3, 5.2]	16.5 [14.9, 18.2]	22.8%	31.0%	167 [6.1%]	57 [2.1%]	3 [0.1%]	12 [0.4%]	42 [1.5%]	47 [1.7%]
Mean				22.3 [18.9, 26.4]	0.5 [0.1, 1.1]	9.0 [7.1, 11.3]	12.7 [10.1, 16.1]	25.3%	28.6%	350 [17.7%]	63 [4.0%]	1 [0.1%]	17 [1.2%]	44 [2.8%]	24 [1.4%]
Weighted mean				16.2 [13.9, 19.1]	0.5 [0.1, 1.1]	5.8 [4.5, 7.2]	10.0 [8.2, 12.2]	17.9%	21.8%	409 [16.9%]	53 [3.0%]	1 [0.1%]	13 [0.8%]	38 [2.1%]	24 [1.2%]
Mean [late summer]				21.4 [18.0, 25.6]	0.5 [0.1, 1.1]	8.6 [6.7, 10.9]	12.3 [9.8, 15.5]	24.4%	28.4%	343 [16.9%]	55 [3.6%]	1 [0.0%]	15 [1.0%]	39 [2.5%]	23 [1.3%]
Weighted mean [lt. s.]				15.0 [12.7, 17.8]	0.5 [0.1, 1.1]	5.3 [4.1, 6.7]	9.2 [7.5, 11.3]	16.4%	21.1%	401 [16.6%]	47 [2.7%]	1 [0.0%]	12 [0.7%]	34 [1.9%]	22 [1.1%]

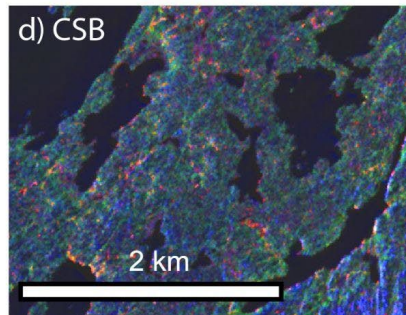
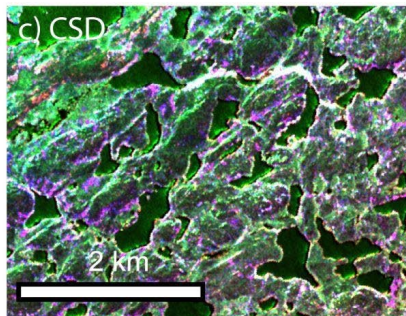
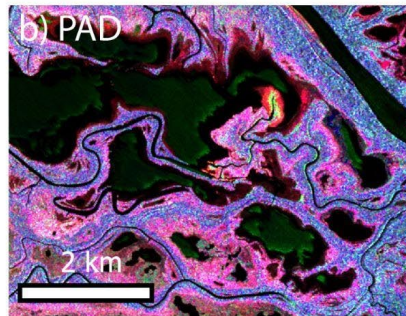
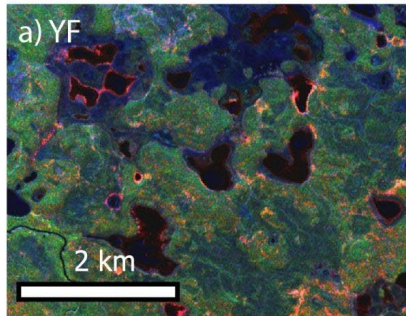
541 **Table 2.** Within-lake emergent vegetation coverages (A_{LEV}) by vegetation type (A_{WF} = area of
542 wet forest, A_{WS} = area of wet shrub, A_{WG} = area of wet graminoid, A_{WEV} = area of wetland
543 emergent vegetation, as opposed to lake vegetation) and by study area, along with landscape
544 coverage in km² and as percent coverages. Numbers in brackets give the bootstrapped 95%
545 confidence intervals. Weighted mean columns are weighted by individual lake area, and
546 summary weighted mean rows are weighted by the total lake area of each study area for all dates
547 and late summer only (August and September, abbreviated as lt. s. when necessary).

548

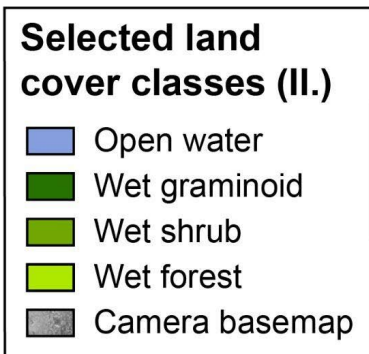
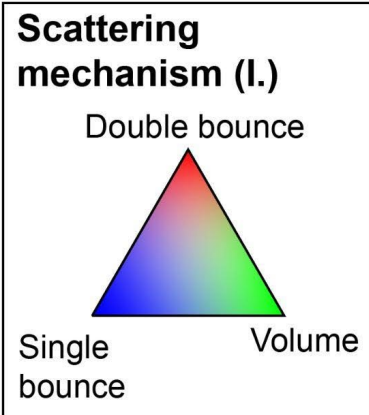
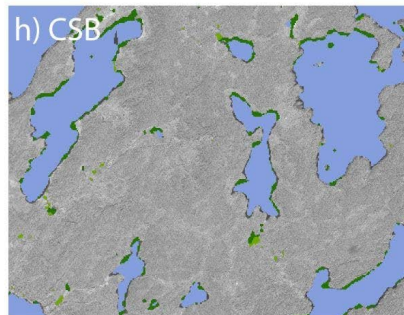
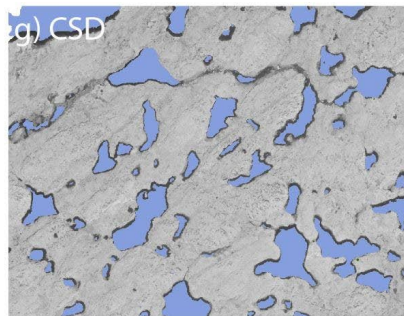
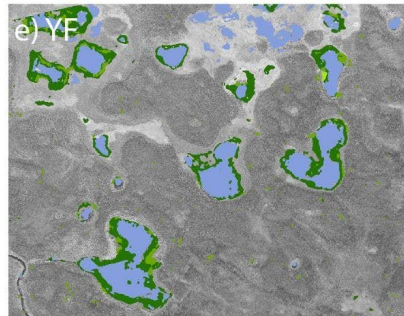
549 3.1.2 Validation of UAVSAR classifier

550 The land cover classifier successfully retrieves the three broad classes of emergent
551 vegetation. Based on visual inspection of the land cover maps, the most significant
552 misclassification is evidenced by false detections of water in areas actually covered by dry
553 graminoid vegetation (**Figure 3e**, top middle) and false detections of inundated vegetation in
554 areas of forest. The most frequent misclassification occurs between Wet Shrub and Rough
555 Water, although errors of omission and commission are roughly equal, implying a near-zero net
556 effect on the landscape totals (**Figure S.1**). Any misclassification among the dry land classes
557 does not affect our lake analysis, and misclassification between the flooded and dry classes is
558 rare, as expected, given the sensitivity of SAR to water presence (**Figure S.1**). Prior to the
559 quality control measures (**Section 2.3.4**), Cohen's kappa coefficients are 0.862 for the model
560 used on the simpler CSD landscape and 0.824 for the model used for the remaining sites,
561 implying good agreement with the validation data. Since the analysis only uses flooded classes
562 connected to open water that could be validated by optical imagery, errors of commission
563 (**Figure S.1**) represent an upper bound.

I. SAR Image



II. Classification



565 **Figure 3.** Example L-band SAR images of subsets within the four study areas (**Column I. a-d**, YF
 566 6/2017, PAD 9/2019, CSD 9/2017, CSB 8/2018, respectively) and corresponding classification
 567 (**Column II. E-h**). SAR images are colorized by Freeman-Durden scattering mechanism (double
 568 bounce in red, primarily indicating emergent vegetation; volume scattering in green, primarily
 569 indicating leafy vegetation; and single bounce scattering in blue, primarily indicating bare
 570 ground, bedrock, and some types of trees) and are stretched identically, with visual adjustments
 571 for brightness and color saturation. In column II., only inundated classes are shown and are

572 superimposed over a grayscale version of the color-infrared camera base map from Kyzivat et al.
573 (2018), in which forests appear darker than grasslands or bedrock.

574

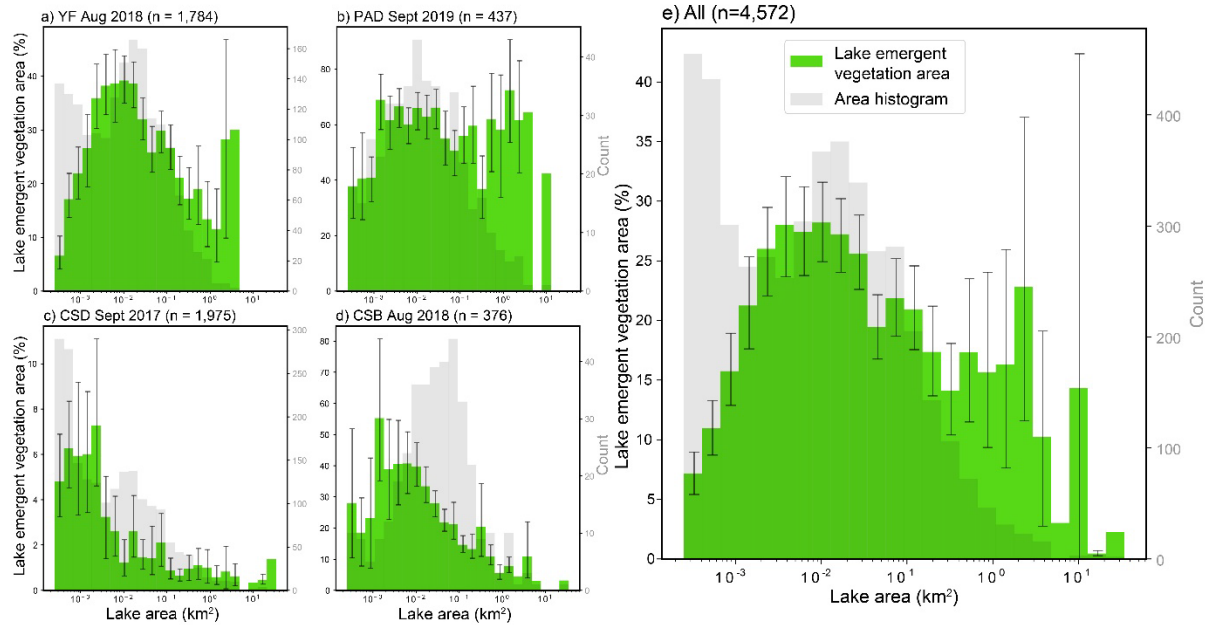
575 3.2 Emergent vegetation extent

576 3.2.1 Regional and morphological trends

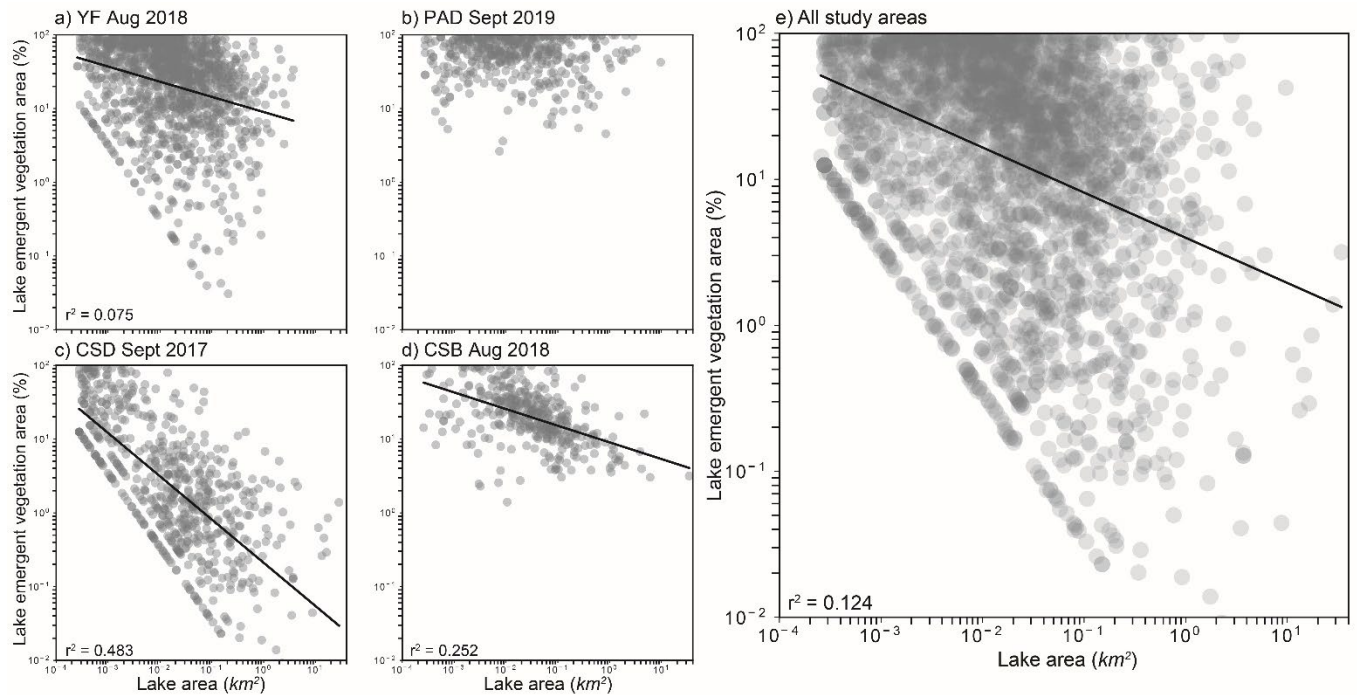
577 Although useful for integrating all flux components, landscape-scale descriptors obscure
578 the nuance of individual lake characteristics. Consequently, we also present results normalized
579 by each lake's area and aggregated via weighted averaging (**Table 2, Figure 4**). With this
580 normalization, it is more apparent that emergent vegetation (A_{LEV}) is quite prevalent in lakes,
581 averaging 16.2 [13.9 – 19.1]% across the four study areas, weighted by lake area. Again,
582 coverage is especially extensive in the lowland PAD and YF (**Figure 2**), averaging 59 [50 –
583 68]% and 22 [20 – 25]%, respectively. A_{LEV} in the more topographically constrained, colder,
584 sparsely vegetated CSB and CSD areas averages 7.0 [4.7 – 11.5]% and 1.0 [0.8 – 1.2]%,
585 respectively. The lowland sites, therefore, have the most A_{LEV} , both as a percentage of total lake
586 area as well as landscape area.

587 While emergent vegetation is observed in every size bin in every area, we find only a
588 weak relationship between A_{LEV} and lake area that holds for all study areas. The area bins
589 comprising small to medium-sized lakes between 0.002 to 0.02 km² always contain the primary
590 histogram peak, with the exception of the PAD, for which these bins contain the secondary peak
591 (**Figure 4b**). In all regions except the PAD, the smallest observable lakes (≥ 250 m²) have
592 similar coverage to the largest (> 10 km²), resulting in unimodal area-binned histograms, even
593 within the confidence intervals (**Figure 4**). The drop in A_{LEV} for small lakes is likely caused by
594 mixed pixels in narrow littoral zones being detected as water. Even so, Pearson correlation is
595 weak between log-transformed A_{LEV} and lake area ($r^2 = 0.124$, $p < 0.001$, **Figure 5**), implying
596 that the inverse relationship between the two variables is not consistent across sites. On an
597 individual basis, the two Canadian Shield study areas have significant regression relationships (p
598 < 0.001 , **Figure 5**), with $r^2 = 0.25$ (CSB) and 0.48 (CSD), likely explained by their simpler,
599 bedrock-dominated landscapes.

600



602 **Figure 4.** Emergent vegetation (A_{LEV}) is most prevalent in small to medium-sized lakes. Here,
 603 mean A_{LEV} , in green, is calculated for logarithmic lake area bins for each region (a) and for all
 604 regions combined (b). Error bars give the 95% confidence interval for A_{LEV} for all bins with > 2
 605 observations. The lake count in each bin is plotted in grey and shows that most observed lakes
 606 are much smaller than 1 km². Accordingly, bins with fewer lakes generally have greater
 607 uncertainty in A_{LEV} , and the rightmost bins, which contain < 10 lakes, have considerable
 608 uncertainty. For a version of this figure showing bin sums, rather than means, see **Figure S.2**.
 609
 610



612 **Figure 5.** Scatter plot of lake area and emergent vegetation coverage (A_{LEV}) for all 4,572 lakes by
 613 study area (a-d) and aggregated (e). There is only a weak relationship between the two log-
 614 transformed variables. The diagonal bottom-left boundary in most plots is caused by area
 615 quantization by pixilation; since A_{LEV} is a fraction, the minimum possible A_{LEV} corresponding to a
 616 one-pixel vegetated zone decreases as the denominator increases. Lakes with $A_{LEV} = 0$ are not
 617 shown nor included in the regression and regression lines are only included for $p < 0.001$.

618 3.2.2 Seasonal trends

619 Despite fluctuating water levels, the distribution of A_{LEV} across lakes of varying areas
 620 remains largely similar across seasons and years (**Figure S.3**). In all study areas, there is a
 621 histogram peak at lakes with little or no emergent vegetation (**Figure S.3 a-d**, leftmost bin), as
 622 many areas lack the necessary conditions to support emergent macrophytes. The histogram drops
 623 sharply with increasing A_{LEV} coverage: extremely quickly in the sparsely-vegetated CSD,
 624 somewhat quickly in the more southern CSB, and gradually in YF. The negative-skewed PAD
 625 distribution (tail on left) is an anomaly with high-coverage lakes common. Accordingly, the area-
 626 weighted mean (58.9 %) is barely greater than the arithmetic mean coverage (58.6 %) in the
 627 PAD, unlike the rest of the study areas and the aggregated total, for which these values can differ
 628 by a factor of two (**Table 2**). There are also more lakes overall detected in the PAD during early
 629 summer (**Figure S.3**), likely because temporarily submerged macrophytes would be detected as
 630 open water and thus constitute lakes in our analysis. These effects are likely due to prevalence of
 631 shallow open water wetlands, which are ubiquitous in the delta and are included in our lake
 632 dataset as long as some area of open water ($> \text{one pixel, or } \sim 30 \text{ m}^2$) is detected. Although there is
 633 little seasonal variance to the A_{LEV} distribution, the corresponding methane fluxes may depend
 634 greatly on plant activity, which varies between seasons. To avoid including seasonal wetlands as
 635 lakes, we used only the late summer (low water season) land cover maps to calculate mean A_{LEV}
 636 and have broken down available flux data by season. The temporal invariance of the A_{LEV}

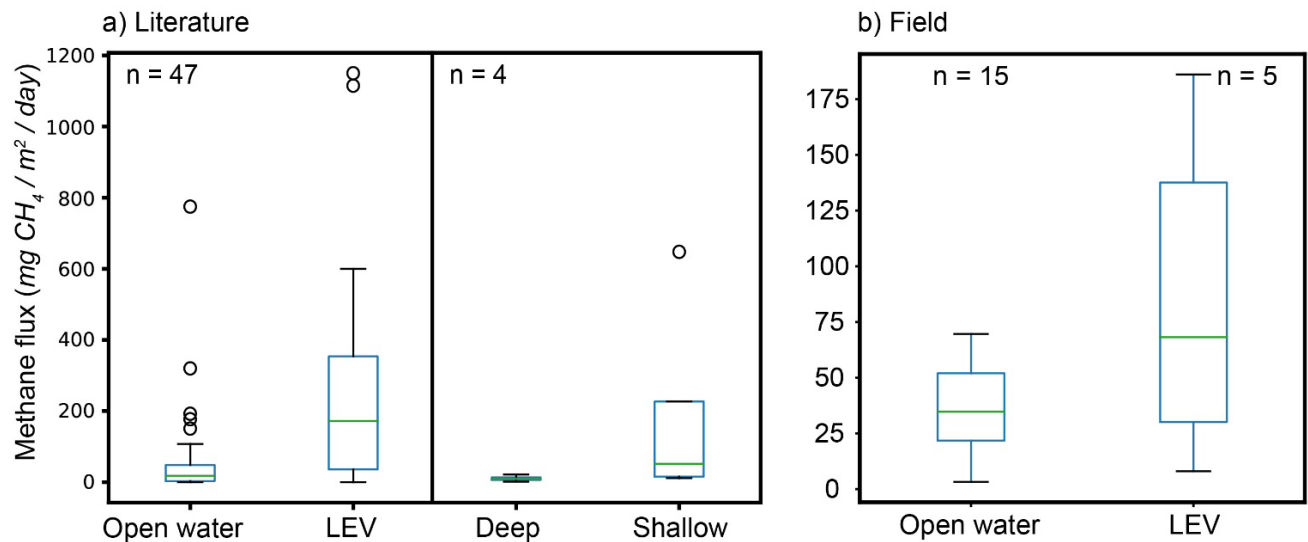
637 histograms provides further validation of the consistency of the classifier, and it shows how
 638 changes in *A_{LEV}* are not relegated to the same small subset of lakes.

639

640 3.3 Methane fluxes from emergent macrophytes vs. open water

641 Field measurements confirm that methane fluxes per unit area from emergent
 642 macrophytes are consistently higher than open water, even within the same lake (**Figure 6**).
 643 Although macrophyte fluxes were only collected at five of the 15 visited PAD lakes, four have
 644 higher mean macrophyte values than open water, leading to a mean macrophyte: open water flux
 645 ratio of 2.3 (Kyzivat et al., 2021b). Given the small sample size, differences are not significant (u
 646 = 2.0, $p = 0.19$, $n = 5$) based on the non-parametric Mann-Whitney test. Strong variability in the
 647 measurement may also contribute, since these short-term measurements exclude ebullition and
 648 the other key episodic open water fluxes (ice-out flux, water column turnover fluxes) are
 649 accounted for afterwards via a correction factor. Similarly, plants, as well as open water, can
 650 have pronounced diel and seasonal variability in their fluxes, and these measurements were all
 651 made during the day.

652 The fluxes obtained by literature synthesis (**Table S.3**) have an even more extreme
 653 median ratio of 8.8 (**Figure 6**; **Figure 7**, top histogram), with a significant difference between
 654 open water and vegetation ($u = 1,800$, $p < 0.001$, $n = 47$). Of the 56 paired vegetation versus
 655 open water measurements, all but eight have flux ratios > 1 , implying greater emissions from
 656 vegetated regions. The PAD and literature measurements combined have a median flux ratio of
 657 6.1, or 15.9 if only Arctic-boreal lakes are included. We use the former, smaller value, since it
 658 comes from a larger sample size, and multiply it by the ice-melt flux correction factor to obtain
 659 4.6, which is used for the subsequent sensitivity calculation (**Table 3**). Due to limited data,
 660 studies from all seasons and measurement periods were used, and some only measured one or
 661 two of the emission pathways (see **2.3.6**). The four studies that defined lake zones based on
 662 depth rather than vegetation yielded a median flux ratio of 15.8. Despite a limited and
 663 spatiotemporally uneven global sampling, lakes in our study areas and worldwide unequivocally
 664 trend towards higher emissions from emergent macrophyte environments than from open water.

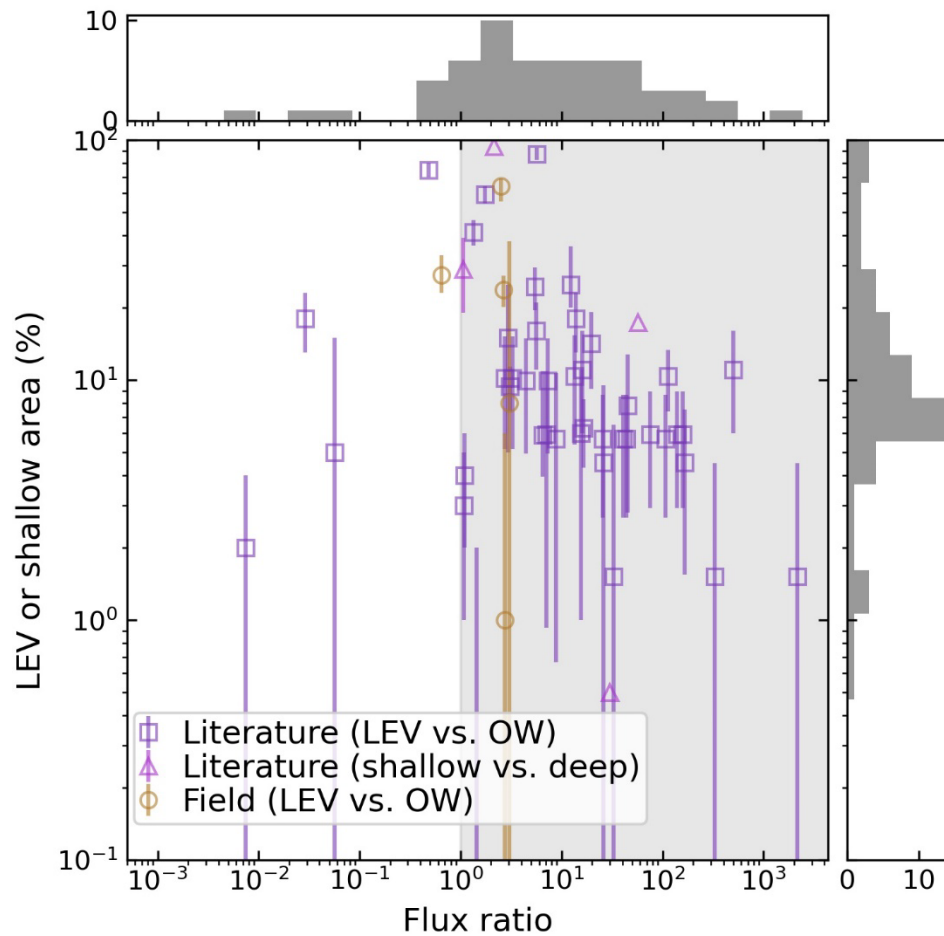


666 **Figure 6.** Lake emergent vegetation (LEV) and shallow regions produce greater methane fluxes
667 than open water zones and deep regions, respectively, based on the literature (a) and from field
668 measurements in the Peace-Athabasca Delta in July and August 2019 (b). Green lines show the
669 median, hinges are drawn at the lower and upper quartiles, and flyer bars give the extent of data
670 not considered outliers, which are plotted as points. Note the different scales demonstrating
671 much greater flux values (mg of CH₄ /day) from the literature (a) than in the PAD (b).

672

673 3.4 Sensitivity of whole-lake methane emissions to inclusion of vegetated areas

674 By applying the median macrophyte: open water ratio of 6.1 (**Figure 7**) to our remotely
675 sensed UAVSAR LEV maps (**Figure 3**), we estimate the relative importance of accounting for
676 emergent vegetation in whole-lake methane flux estimates (**Table 3**). Assuming a lake area
677 weighted average A_{LEV} of 16.2 [13.9 - 19.1]% increases the overall methane emissions from the
678 four study areas by 21 [18 - 25]% (**Figure 7**). Although the flux ratio R' has variability, we have
679 not included it within the bounds of the estimate, relying instead on the more robust
680 measurement of variance of A_{LEV} . When re-normalized to total inland aquatic emissions (lakes,
681 reservoirs, rivers, wetlands, **Equations 3**), the modified impact, I' , is 5 [4-6]%.
682 Spatiotemporally, the impact ratio I varies from 4% to 321%, with the lower bound coming from
683 CSD in September 2017 (where only ~0.9% of lake areas contains emergent vegetation) and the
684 upper bound from the PAD in June 2017 (~66% coverage, **Table 2**). Although these are the most
685 extreme values observed, these scenarios show that accounting for small, but numerous LEV
686 zone areas significantly raises whole-lake emissions estimates.



688 **Figure 7.** Plotting study lakes in a flux ratio-emergent vegetation fraction feature space shows
 689 that most would have higher calculated fluxes (shaded area) if their lake emergent vegetation
 690 (LEV) zones are accounted for separately from open water, with median increase of 21%.
 691 Studies that partitioned fluxes into shallow versus deep, rather than vegetated vs. open water
 692 zones are plotted with triangular markers, but are not used for further analysis. The distributions
 693 of both variables are shown as histograms along the relevant axes. Vertical error bars show the
 694 temporal range in coverage for the field data (orange circles) and the estimated mapping
 695 uncertainty for the literature data (purple squares) and can extend to zero (beyond axis limits).
 696 For scale, the uppermost square data point in the figure (peat pond, Ontario, Canada)
 697 corresponds to a 113% increase in emissions compared to the no LEV zone case. Note the

698 logarithmically-scaled x and y axes. For a version of this figure with contour lines showing how
699 much higher this calculated flux would be, see **Figure S.4.4**.

700

<i>A_{LEV}</i>	<i>c</i>	<i>R</i>	<i>R'</i>	<i>I</i>	<i>I'</i>
16.2 [13.9 – 19.1]%	0.36	6.1	4.6	21 [18-25]%	5 [4-6]%

701 **Table 3.** Parameters and results of sensitivity calculation (**Equations 2 and 3**). *A_{LEV}* is area, with
702 95% confidence intervals, of lake emergent vegetation and is corrected for double-counting with
703 wetlands by the scalar *c*. *R* is the median global vegetated: open water flux ratio obtained from
704 the literature and is adjusted to *R'* correct for unmeasured ice-melt fluxes. The results *I* and *I'*
705 represent the impacts of accounting for LEV in whole-lake methane flux estimates, normalized
706 by total lake (assumed open water) and total inland aquatic area (lakes, reservoirs, rivers,
707 wetlands), respectively.

708 4 Discussion and Conclusion

709 4.1 Emergent vegetation coverage in lakes

710 Littoral zones are often theorized to cover greater portions of small lakes than large
711 (Bergström et al., 2007; Wetzel, 1990, 2001). It is logical that smaller lakes with larger
712 perimeter: area ratios would be dominated by near-shore areas, which are overwhelmingly
713 shallow. However, while our results generally show greater fractional emergent vegetation area
714 (*A_{LEV}*) in small and medium-sized lakes (**Figure 4**), there is weak correlation at best (Pearson $r^2 =$
715 0.124, $p < 0.001$; **Figure 5**). This discrepancy can likely be explained by lake emergent
716 vegetation (LEV) comprising only a portion of the littoral zone, as well as mixed pixels
717 obscuring narrow littoral margins in small lakes. Bergström et al. (2007) similarly observed that
718 medium-sized lakes (0.1 to 1 km²) had the greatest *A_{LEV}* of ~11% on average for 50
719 Fennoscandian Shield lakes in Finland, which, plotted as an area-binned histogram, also
720 resembles an inverted V-shaped curve. Mäkelä et al (2004), using the same dataset, pointed out
721 that large, lowland lakes had the largest total macrophyte coverage, also noting that area and pH
722 only account for 15% variation in *A_{LEV}*.

723 In comparison, the Canadian Shield areas we sampled contained the greatest *A_{LEV}* in
724 small-to-medium lakes (0.0001 - 0.002 km² in area), with values ranging from 7.3 [4.5 – 10.7] %
725 (CSD) to 55 [35 – 81] % (CSB). We also observe a large contribution to total *A_{LEV}* from the large
726 lakes (**Figure S.2**), underscoring the need not to discount them. Incidentally, these lakes are
727 under-represented in lake methane datasets (Deemer & Holgerson, 2021). The largest 100 lakes
728 (area ≥ 0.9 km²) comprise 62.7% of total lake area and 39.2% of total LEV area across all four
729 study areas, and this trend holds across all study areas (**Fig S.2**). The observed region-specific
730 dependence on lake area further highlights the need for remote sensing to estimate littoral or
731 vegetated zone coverage as well as to identify the interface between wetlands and open waters in
732 the context of aggregated methane emission estimates.

733 The ~16% mean *A_{LEV}* coverage we observe is greater than the globally-inclusive estimate
734 of 7% (Duarte et al., 1986) and Southern Finland estimate of 5.2% (Bergström et al., 2007). Since

735 the number is an intermediate average derived from much lower values on the Canadian Shield
736 (1.0%, and 7.0% for CSD and CSB, respectively, **Table 2**) and much higher values for the PAD
737 (59%) and YF (22%), it is highly sensitive to the choice of study areas and their relative sizes.
738 Even though the relationship between coverage and lake area does not appear as simple as
739 suggested by Duarte et al. (1986), their conclusion that lake area is not a strong predictor of
740 emergent macrophyte coverage is still supported. Although the Boreal–Arctic Wetland and Lake
741 Dataset (BAWLD; Olefeldt et al., 2021a; Olefeldt et al., 2021b) does not explicitly map littoral
742 vegetation, the authors defined all open-water ecosystems as lakes, which includes shallow open-
743 water wetlands. As a result, their lake class is defined nearly identically to ours, and they cite
744 similar reasons regarding the importance emergent macrophytes as controls on net emissions.
745 Indeed, comparison between datasets shows similar (ranging from 3-46% difference) lake
746 coverage in each study area and an identical area-weighted mean over all study areas (16.6%,
747 **Table S.6**). The roughly equivalent emergent vegetation and/or wetland classes are 24% greater
748 in BAWLD (3.8% areal coverage from UAVSAR, 4.7% from BAWLD), which indicates that
749 some or all LEV is included within BAWLD wetlands. BAWLD therefore represents best
750 practices not only in ensuring a consistent lake-wetland distinction, but also presumably in
751 including lake emergent vegetation within a wetland class, where it can be assigned a more
752 appropriate methane flux.

753 4.2 Importance of emergent vegetation for methane upscaling

754 4.2.1 Toward improved upscaling of lake methane emissions

755 This broad-domain study supports previous studies demonstrating the importance of
756 accounting for vegetated and/or littoral areas in upscaling lake methane flux estimates
757 (Bergström et al., 2007; Casas-Ruiz et al., 2021; DelSontro et al., 2018a; Juutinen et al., 2003;
758 Kankaala et al., 2013; Natchimuthu et al., 2016; Smith & Lewis, 1992; Striegl &
759 Michmerhuizen, 1998). However, in addition to the challenges of measuring wetland extent
760 more generally (Melton et al., 2013), a knowledge gap remains about the distribution and area of
761 lake littoral zones (Huttunen et al., 2003). Our airborne UAVSAR approach for detecting lake
762 emergent vegetation (LEV) has limited spatial coverage and is unsuitable for broader-scale
763 studies. Satellite approaches, however, have good utility for pan-Arctic or global wetland
764 mapping (Hess et al. 1990, Nelson et al. 2006, Ghirardi et al. 2019, Zhang et al. 2021) and are
765 well suited for study of large lakes, which contribute most to total LEV area (**Fig S.2**). These
766 lakes are otherwise considered low methane emitters on a per-area basis (Holgerson & Raymond,
767 2016) and have little risk of being double-counted in wetland datasets, so they would be a good
768 starting point for future studies. Incidentally, DelSontro et al. [2018] define an underestimation
769 ratio between pelagic and littoral methane concentrations (roughly the inverse of I) and show that
770 it approaches unity for larger lakes, although they do not calculate the impact of these lakes to
771 total lake emissions. The upcoming NISAR satellite mission is likely to provide high-resolution,
772 freely available global coverage of L-band SAR, which may facilitate similar analysis for *A_{LEV}*
773 over larger scales.

774 Unfortunately, our results do not reconcile the gap between modeled methane fluxes from
775 bottom-up and top-down models (Thornton et al. 2016; Saunois et al., 2020). In fact, they
776 suggest bottom-up fluxes are slightly greater than previously thought, which further widens the
777 discrepancy. The most recent aquatic upscaling studies (Saunois et al., 2020; Rosentreter et al.,
778 2021) and a recent wetland synthesis dataset for modeling [(Zhang et al., 2021)], used a

779 consistent lake mask when defining lake and wetland areas, and this careful lake masking has not
780 significantly improved the discrepancy (Saunois et al., 2020). These masks either come from
781 global lake datasets (HydroLakes, GLWD, GLOWABO), or the more recent global surface water
782 explorer (GSW). Both GLOWABO and GSW were derived from 30 m resolution, optical
783 Landsat satellite data, which is quite effective at detecting open water. It is unclear whether these
784 methodologies include vegetation as part of lakes, although GLOWABO and HydroLakes show
785 good agreement with our open water class (**Table S.4**). Wetland detection is more challenging
786 and hampered by scale disparities between the relevant satellite sensors and inconsistent wetland
787 definitions between disciplines ([Poulter et al., 2017]; Zhang et al., 2021). Thus, the practice of
788 using consistent open-water lake masks to differentiate between lakes and wetlands is a good
789 one.

790 Our results show that even after correcting for double-counted wetlands, UAVSAR
791 detects emergent vegetation in 5.8% of lakes contained in global datasets. Whether through
792 temporal change or dissimilar mapping methods, this discrepancy is large enough to have an
793 impact on the lake methane budget. Equally important, but not demonstrated here, is accounting
794 for the uniquely high emissions from non-vegetated lake littoral zones, which are less likely to be
795 confused with wetlands, and are probably at least as extensive as LEV (Seekell et al., 2021).
796 Non-vegetated littoral zones can also be high emitters, especially when within the reach of
797 carbon-exuding roots and rhizomes (Bansal et al. 2020). Since mapped LEV falls within littoral
798 zones by definition, it shares some of their properties, but our analysis does not attempt to
799 separate these drivers. It is likely that another positive correction could be made littoral zones
800 with submerged, floating-leafed or no vegetation, for which there is even less comparison data.
801 Given that our LEV flux data includes all emission pathways in a variety of lake types, the
802 resulting flux ratios represent a combination of many correlated drivers, including shallowness,
803 methane oxidation, variable inundation, proximity to terrestrial inputs, and microbial community.
804 In the context of deriving spatially explicit representations of methane emissions, it could be
805 preferable to move away from using discrete land cover classes, and develop continuous
806 representations of the processes that control methane production and rates of flux. These
807 representations could better describe gradually-varying conditions, such as water table depth, the
808 resulting concentration of oxygen in the subsurface, and the inclusion of new estimates of soil
809 moisture, and they could improve estimates of methane emissions along hydrologic gradients.

810

811 4.2.2 Limitations and future directions

812 Our 21% estimate for I (**Equation 2**), the percent increase due to including emergent
813 vegetation in lake methane flux accounting, uses assumptions chosen to lead to the smallest
814 possible value. Regardless, it is highly sensitive to the data-limited input parameters c and the
815 flux ratio, which has a large variability that we have not accounted for. The double-counting
816 correction factor c may suffer from lack of generality, since it was calculated only within the
817 boundaries of our study regions using global datasets collected ~ 20 years prior. It also assumes
818 that LEV zones have similar areal emission to wetlands, which may not be valid. Clearly, more
819 methane flux measurements in shallow or vegetated zones and estimates of total macrophyte
820 coverage are needed (Bergström et al., 2007; Schmiedeskamp et al., 2021). While our approach
821 for correcting for double counting is only based on lakes large enough to be included in global
822 datasets, the small magnitude of c shows how easy it is to count wetlands as LEV. Without this

823 correction factor, I would be more than doubled to 58%. Future work should look more
824 generally at the cause and magnitude of lake/wetland double counting (Thornton et al., 2016) and
825 develop continuous metrics for methane emission habitats that don't rely on discrete land cover
826 classes.

827 Our estimate for I may still be too high because our A_{LEV} includes up to 2.6% emergent
828 shrubs and trees, even after the double-counting correction (**Table S.5**). This woody vegetation
829 lacks the aerenchyma tissue that allows most wetland plants to transport methane from the
830 sediments. Recent work has shown the potential for microbes living inside trees to produce
831 methane (Covey & Megonigal, 2019), although this effect is likely less than soil microbe
832 production. Secondly, the relatively narrow swath width of UAVSAR causes large (and likely
833 less-vegetated) lakes to be under-represented in the calculation of weighted mean A_{LEV} . Adding
834 to this effect is the use of the same vegetated: open water ratio for lakes of all sizes, when
835 smaller lakes and ponds are known to be higher open-water methane emitters than large
836 (Michmerhuizen, Striegl, & McDonald, 1996; Bastviken et al., 2004; Holgerson & Raymond,
837 2016; Engram et al. 2020), probably because littoral zones (vegetated and unvegetated) cover
838 most of their areas. Indeed, Kankaala et al. (2013) showed that the flux ratio increases with lake
839 size. It follows that our concept of a vegetated: open water flux ratio is less useful for small lakes
840 and would likely be even larger for the largest lakes, which were under-represented in our
841 literature synthesis. Future studies could better quantify how this ratio varies based on lake area.
842 Nevertheless, since the contribution to total A_{LEV} from the small lakes is so slight (**Fig S.2**), they
843 don't have a large negative impact on our estimate. Finally, the estimate compares to a
844 hypothetical upscaling using solely open water fluxes, while in reality, some studies include
845 open-water measurements from littoral zones. While many of the studies cited here used area-
846 weighted approaches with regard to lake depth zones (Natchimuthu et al., 2016; DelSontro et al,
847 2016), they appear to be a minority and are not available on the global scale (Kuhn et al. 2021b;
848 Wik et al. 2016b).

849 Comparison of our sensitivity study with previous Arctic-boreal and global lake studies
850 suggests that our finding of a 21% increase in whole-lake methane flux is conservative. Using
851 flux chamber measurements from two Swedish lakes, Natchimuthu et al. (2016) found that
852 methane emissions from lake centers are 2.1 times smaller than whole-lake fluxes, although
853 fluxes were not explicitly measured near lake macrophytes. Similarly, Kankaala et al. (2013)
854 found that 74-82% of diffusive and plant-mediated emissions in 12 Finnish lakes derived from
855 littoral macrophyte stands comprising only 5% of their total area. These amounts correspond to a
856 flux ratio of 54-86, leading to an impact, I , on whole-lake fluxes between 270 and 430% greater
857 than a case where open water fluxes were assumed throughout. Most recently, Desrosiers et al.
858 (2022) found that the 26% of a boreal lake covered in macrophytes was responsible for 81% of
859 its carbon emissions. The impact of considering the *Typha latifolia* stands alone can be
860 calculated at 102%. Although focused only on extremely high-emitting lake and wetland
861 thermokarst hot spots, Elder et al. (2021) conducted a study of remotely-sensed methane "hot
862 spot" emissions across a 70,000 km² Arctic-boreal domain and found an even greater
863 disproportionality, where 0.005% of the domain was estimated to emit 0.3-16.2 % of the total.
864 The higher reported flux ratios from lake studies can be partly attributed to area-weighted
865 analyses including much larger, and thus lower-emitting per unit area, lakes than our airborne-
866 based study. Yet, they also underscore the pitfalls of assigning higher areal fluxes to vegetated
867 lake zones without ensuring these zones are not otherwise counted as wetlands.

868 Even when using best practices to avoid double-counting lakes with wetlands, the coarse
869 resolution of global lake maps can still cause uncertainty in the precise location of shorelines. At
870 the medium resolution of Landsat (30 m), the entire littoral zone could be “hidden” inside of
871 mixed pixels at lake boundaries, even for large lakes, if they have steep margins. If only unmixed
872 pixels are classified as lakes, it is unclear how near-shore land pixels would be treated, especially
873 given that global wetland maps are typically made from coarser-resolution sensors (Zhang et al.,
874 2021). Unfortunately, this hard-to-resolve small strip of land/water interface is precisely the area
875 with the greatest impact on full-lake (DelSontro et al. 2018, Thornton et al. 2016) and landscape
876 (Elder et al. 2021) fluxes, so it cannot be rounded off. Furthermore, due to changing inundation
877 and vegetation coverage, lakes can contain LEV even if attempts are made to exclude it, such as
878 from static lake maps. Littoral zones often have fluctuating inundation, and there are valid
879 reasons to count them as either lakes or wetlands, even though current upscaling efforts require
880 making this distinction. Just as with wetlands, lakes can be defined differently across disciplines.
881 Although plant-mediated emissions are often reported in studies focused on lakes, upscaling
882 studies frequently exclude vegetated areas from their lake estimates (Bastviken et al., 2011; Wik
883 et al., 2013; Olefeldt et al., 2021a; Rosentreter et al., 2021), a best practice to avoid double-
884 counting. This exclusion requires careful treatment of the fluxes from which “lake” estimates
885 should be derived. Future work should develop techniques that can more accurately measure
886 littoral zone area (Seekell et al., 2021), produce consistent and methane-relevant lake versus
887 wetland criteria from remote sensing (Olefeldt et al., 2021a), and make use of temporally-
888 dynamic inundation maps (Pekel et al., 2016; Zhang et al., 2021) for both wetlands and lakes.

889 Estimating Arctic-boreal lake methane emissions is constrained by limited data and
890 reliance on assumptions such as discrete land cover classes. As noted by Saunio et al. (2020),
891 methane upscaling can be improved by considering spatiotemporal variability and increasing
892 sampling efforts in lakes with diverse morphologies and environmental conditions. Previous
893 estimates have calculated a high bias caused by most measurements being made during waking
894 hours (Sieczko et al., 2020) or summertime sampling (Wik et al., 2016a; Denfeld et al., 2018;
895 Jansen et al., 2020); or from static inundation maps (Hondula et al., 2021). Others have shown
896 low biases from insufficient seasonal (Wik et al., 2016b), or spatial (Wik et al., 2016b;
897 Natchimuthu et al., 2016; Desrosiers et al., 2021) sampling. This study also suggests a low bias
898 from not separately accounting for LEV, on par with the contribution of under-sampled ice melt
899 flux, which ranges from 23 to 27%. Even so, inadequate and geographically-uneven sampling of
900 the world’s > 117 million lakes (Verpoorter et al., 2014) is likely the greatest source of
901 uncertainty in lake upscaling. In the absence of sufficient data, upscaling estimates should make
902 use of available quantitative corrections and continue to find and remediate sampling biases.

903 4.3 Conclusion

904 Lake emergent vegetation (LEV) is ubiquitous in Northern lakes but limited data prohibit
905 its inclusion in upscaling lake methane emissions. We provide a first assessment of its
906 prevalence across 4,572 lakes in four Arctic-boreal regions using airborne UAVSAR mapping
907 and find that they cover 16.2 [13.9 – 19.1]% of Arctic-boreal lakes on average, a higher amount
908 than other estimates, but with strong differences between study areas. LEV is greatest in lowland
909 riverine areas, where changing water levels cause seasonal variability. Consistent with previous
910 studies, we find that it is more common in small than large lakes, but this relationship is weak
911 and varies regionally. Accounting for LEV, using a synthesis of paired open water and LEV field
912 measurements of methane flux, leads to an upscaling estimate 21 [18 - 25]% greater than an

913 estimate that assigns the same open water flux to the entire lake. We conclude that remote
914 sensing of littoral zones, based on vegetation or otherwise, and collection of flux data from all
915 parts of a lake are necessary for accurate upscaling of lake methane emissions. Future studies
916 should continue using consistent definitions to separate lakes and wetlands, incorporate temporal
917 wetland and lake change into analyses, remain vigilant against double counting with wetlands,
918 and use multiple lake zones or continuous metrics for upscaling.

919

920 **Acknowledgments**

921 We thank Robert and Barbara Grandjambe for guiding services; Queenie Gray and Wood
922 Buffalo National Park for enabling our field visits; Alex Shapiro of Alaska Land Exploration
923 LLC for helicopter piloting; the U.S. Fish and Wildlife Service, the Gwichyaa Zhee Gwich'in
924 Tribal Government and Doyon Limited for access to Yukon Flats National Wildlife Refuge;
925 Michael W. Denbina for assistance with UAVSAR data processing; and Kevin Timoney for
926 assistance with botanical identifications;. Field work was conducted on or near land belonging to
927 the Athabasca-Chipewyan, Mikisew Cree, Métis, and Gwich'in indigenous peoples. Resources
928 supporting this work were provided by the NASA High-End Computing (HEC) Program through
929 the NASA Center for Climate Simulation (NCCS) at Goddard Space Flight Center via the
930 ABoVE Science Cloud. UAV Orthomosaics were created using DroneDeploy software. Data
931 processing was made possible in part by the free and open-source software, including python,
932 numpy, pandas, as well as with PolSAR Pro v5.1, which is provided by the European Space
933 Agency (ESA). Any use of trade, firm, or product names is for descriptive purposes only and
934 does not imply endorsement by the U.S. Government. Thanks to Lawrence Vulis and two
935 anonymous reviewers who have greatly improved the manuscript.

936 **Funding**

937 This work was funded by the following NASA programs; Future Investigators
938 in NASA Earth and Space Science and Technology (FINESST), grant number
939 80NSSC19K1361, managed by Dr. Allison Leidner; Terrestrial Ecology Program Arctic-Boreal
940 Vulnerability Experiment (ABoVE), grant number 80NSSC19M0104, managed by Dr. Hank
941 Margolis; and the NASA Surface Water and Ocean Topography mission, grant number
942 NNX16AH83G, managed by Dr. Nadya Vinogradova Shiffer. USGS LandCarbon Program
943 provided funding for KPW, RGS, MMD, and FGT.

944 **Data and software availability**

945 UAVSAR data used for this study can be downloaded at
946 <https://doi.org/10.5067/7PEQV8SVR4DM>. The derivative land cover maps and lake emergent
947 vegetation shapefiles can be found at the accompanying data publication:
948 <https://doi.org/10.3334/ORNLDAAAC/1883>. Methane flux data from the PAD can be found at
949 <https://doi.org/10.6073/pasta/1e0cadadd8024c8fab692ee21dc1f57>. All MATLAB, Python and
950 shell scripts used in data processing can be found at <https://doi.org/10.5281/zenodo.5974901> and
951 <https://doi.org/10.5281/zenodo.5974915>.

952 **References**

- 953 Ayoub, F., Jones, C. E., Lamb, M. P., Holt, B., Shaw, J. B., Mohrig, D., & Wagner, W. (2018).
 954 Inferring surface currents within submerged, vegetated deltaic islands and wetlands from
 955 multi-pass airborne SAR. *Remote Sensing of Environment*, *212*, 148–160.
 956 <https://doi.org/10.1016/j.rse.2018.04.035>
- 957 Bansal, S., Johnson, O. F., Meier, J., & Zhu, X. (2020). Vegetation Affects Timing and Location
 958 of Wetland Methane Emissions. *Journal of Geophysical Research: Biogeosciences*, *125*(9),
 959 e2020JG005777. <https://doi.org/10.1029/2020JG005777>
- 960 Bastviken, D., Cole, J., Pace, M., & Tranvik, L. (2004). Methane emissions from lakes:
 961 Dependence of lake characteristics, two regional assessments, and a global estimate. *Global*
 962 *Biogeochemical Cycles*, *18*(4), 1–12. <https://doi.org/10.1029/2004GB002238>
- 963 Bastviken, D., Tranvik, L. J., Downing, J. A., Crill, P. M., & Enrich-Prast, A. (2011). Freshwater
 964 Methane Emissions Offset the Continental Carbon Sink. *Science*, *331*(6013), 50–50.
 965 <https://doi.org/10.1126/SCIENCE.1196808>
- 966 Bergström, I., Mäkelä, S., Kankaala, P., & Kortelainen, P. (2007). Methane efflux from littoral
 967 vegetation stands of southern boreal lakes: An upscaled regional estimate. *Atmospheric*
 968 *Environment*, *41*, 339–351. <https://doi.org/10.1016/J.ATMOSENV.2006.08.014>
- 969 Bourgeau-Chavez, L. L., Endres, S., Powell, R., Battaglia, M. J., Benschoter, B., Turetsky, M., ...
 970 Banda, E. (2017). Mapping boreal peatland ecosystem types from multitemporal radar and
 971 optical satellite imagery. *Canadian Journal of Forest Research*, *47*(4), 545–559.
 972 <https://doi.org/10.1139/cjfr-2016-0192>
- 973 Bourgeau-Chavez, L. L., Graham, J. A., Endres, S., French, N. H. F., Battaglia, M., Hansen, D.,
 974 & Tanzer, D. (2019). ABoVE: Ecosystem Map, Great Slave Lake Area, Northwest
 975 Territories, Canada, 1997-2011 (Version 1). ORNL Distributed Active Archive Center.
 976 <https://doi.org/10.3334/ORNLDAAAC/1695>
- 977 Bridgham, S. D., Cadillo-Quiroz, H., Keller, J. K., & Zhuang, Q. (2013). Methane emissions
 978 from wetlands: biogeochemical, microbial, and modeling perspectives from local to global
 979 scales. *Global Change Biology*, *19*(5), 1325–1346. <https://doi.org/10.1111/gcb.12131>
- 980 Brown, J., Ferrians, O., Heginbottom, J. A., and Melnikov E. (2002). Circum-Arctic Map of
 981 Permafrost and Ground-Ice Conditions, Version 2 [Data set]. NSIDC.
 982 <https://doi.org/10.7265/SKBG-KF16>
- 983 Burger, M., Berger, S., Spangenberg, I., & Blodau, C. (2016). Summer fluxes of methane and
 984 carbon dioxide from a pond and floating mat in a continental Canadian peatland.
 985 *Biogeosciences*, *13*(12), 3777–3791. <https://doi.org/10.5194/bg-13-3777-2016>
- 986 Casas-Ruiz, J. P., Jakobsson, J., & Giorgio, P. A. del. (2021). The role of lake morphometry in
 987 modulating surface water carbon concentrations in boreal lakes. *Environmental Research*
 988 *Letters*, *16*(7), 074037. <https://doi.org/10.1088/1748-9326/AC0BE3>

- 989 Casper, P., Maberly, S. C., Hall, G. H., & Finlay, B. J. (2000). Fluxes of methane and carbon
990 dioxide from a small productive lake to the atmosphere. *Biogeochemistry*, 49(1), 1–19.
991 <https://doi.org/10.1023/A:1006269900174>
- 992 Cheng, X., Huang, W., & Gong, J. (2014). Improved van Zyl polarimetric decomposition
993 lessening the overestimation of volume scattering power. *Remote Sensing*, 6(7), 6365–
994 6385. <https://doi.org/10.3390/rs6076365>
- 995 Christensen, T. R., Panikov, N., Mastepanov, M., Joabsson, A., Stewart, A., Öquist, M., ...
996 Svensson, B. (2003). Biotic controls on CO₂ and CH₄ exchange in wetlands – a closed
997 environment study. *Biogeochemistry*, 64(3), 337–354.
998 <https://doi.org/10.1023/A:1024913730848>
- 999 Colmer, T. D. (2003). Long-distance transport of gases in plants: a perspective on internal
1000 aeration and radial oxygen loss from roots. *Plant, Cell and Environment*, 26(1), 17–36.
1001 <https://doi.org/10.1046/j.1365-3040.2003.00846.x>
- 1002 Covey, K. R., & Megonigal, J. P. (2019). Methane production and emissions in trees and forests.
1003 *New Phytologist*, 222(1), 35–51. <https://doi.org/10.1111/NPH.15624>
- 1004 Dacey, J. W. H., & Klug, M. J. (1979). Methane efflux from lake sediments through water lilies.
1005 *Science*, 203(4386), 1253–1255. <https://doi.org/10.1126/science.203.4386.1253>
- 1006 Deemer, B. R., & Holgerson, M. A. (2021). Drivers of Methane Flux Differ Between Lakes and
1007 Reservoirs, Complicating Global Upscaling Efforts. *Journal of Geophysical Research:*
1008 *Biogeosciences*, 126(4), e2019JG005600. <https://doi.org/10.1029/2019JG005600>
- 1009 DelSontro, T., Boutet, L., St-Pierre, A., del Giorgio, P. A., & Prairie, Y. T. (2016). Methane
1010 ebullition and diffusion from northern ponds and lakes regulated by the interaction between
1011 temperature and system productivity. *Limnology and Oceanography*, 61(S1), S62–S77.
1012 <https://doi.org/10.1002/lno.10335>
- 1013 DelSontro, T., Beaulieu, J. J., & Downing, J. A. (2018a). Greenhouse gas emissions from lakes
1014 and impoundments: Upscaling in the face of global change. *Limnology and Oceanography*
1015 *Letters*, 3(3), 64–75. <https://doi.org/10.1002/lol2.10073>
- 1016 DelSontro, T., del Giorgio, P. A., & Prairie, Y. T. (2018b). No Longer a Paradox: The
1017 Interaction Between Physical Transport and Biological Processes Explains the Spatial
1018 Distribution of Surface Water Methane Within and Across Lakes. *Ecosystems*, 21(6), 1073–
1019 1087. <https://doi.org/10.1007/s10021-017-0205-1>
- 1020 Denfeld, B. A., Baulch, H. M., del Giorgio, P. A., Hampton, S. E., & Karlsson, J. (2018). A
1021 synthesis of carbon dioxide and methane dynamics during the ice-covered period of
1022 northern lakes. *Limnology and Oceanography Letters*, 3(3), 117–131.
1023 <https://doi.org/10.1002/LOL2.10079>
- 1024 Desrosiers, K., DelSontro, T., & del Giorgio, P. A. (2022). Disproportionate Contribution of
1025 Vegetated Habitats to the CH₄ and CO₂ Budgets of a Boreal Lake. *Ecosystems* 2021, 1–20.

- 1026 <https://doi.org/10.1007/S10021-021-00730-9>
- 1027 Dove, A., Roulet, N., Crill, P., Chanton, J., & Bourbonniere, R. (1999). Methane dynamics of a
1028 northern boreal beaver pond. *Ecoscience*, 6(4), 577–586.
- 1029 Duarte, C. M., Kalff, J., Peters, R. H., & Peters, R. H. (1986). Patterns Biomass and Cover of
1030 Aquatic Macrophytes in Lakes. *Canadian Journal of Fisheries and Aquatic Sciences*, 43,
1031 1900–1908.
- 1032 Elder, C. D., Thompson, D. R., Thorpe, A. K., Chandanpurkar, H. A., Hanke, P. J., Hasson, N.,
1033 James, S. R., Minsley, B. J., Pastick, N. J., Olefeldt, D., Anthony, K. M. W., & Miller, C. E.
1034 (2021). Characterizing Methane Emission Hotspots From Thawing Permafrost. *Global*
1035 *Biogeochemical Cycles*, 35(12), e2020GB006922. <https://doi.org/10.1029/2020GB006922>
- 1036 Engram, M., Walter Anthony, K. M., Sachs, T., Kohnert, K., Serafimovich, A., Grosse, G., &
1037 Meyer, F. J. (2020). Remote sensing northern lake methane ebullition. *Nature Climate*
1038 *Change*, 10(6), 511–517. <https://doi.org/10.1038/s41558-020-0762-8>
- 1039 Freeman, A., & Durden, S. L. (1998). A three-component scattering model for polarimetric SAR
1040 data. *IEEE Transactions on Geoscience and Remote Sensing*.
1041 <https://doi.org/10.1109/36.673687>
- 1042 Ganju, N. K., Defne, Z., Kirwan, M. L., Fagherazzi, S., D’Alpaos, A., & Carniello, L. (2017).
1043 Spatially integrative metrics reveal hidden vulnerability of microtidal salt marshes. *Nature*
1044 *Communications* 2017 8:1, 8(1), 1–7. <https://doi.org/10.1038/ncomms14156>
- 1045 Ghirardi, N., Bolpagni, R., Bresciani, M., Valerio, G., Pilotti, M., & Giardino, C. (2019).
1046 Spatiotemporal dynamics of submerged aquatic vegetation in a deep lake from sentinel-2
1047 data. *Water*, 11(3), 1–14. <https://doi.org/10.3390/w11030563>
- 1048 Hastie, A., Lauerwald, R., Weyhenmeyer, G., Sobek, S., Verpoorter, C., & Regnier, P. (2018).
1049 CO2 evasion from boreal lakes: Revised estimate, drivers of spatial variability, and future
1050 projections. *Global Change Biology*, 24(2), 711–728. <https://doi.org/10.1111/GCB.13902>
- 1051 Hess, L. L., Melack, J. M., & Simonett, D. S. (1990). Radar detection of flooding beneath the
1052 canopy a review. *International Journal of Remote Sensing*, 11(7), 1313–1325.
- 1053 Holgerson, M. A., & Raymond, P. A. (2016). Large contribution to inland water CO2 and CH4
1054 emissions from very small ponds. *Nature Geoscience*, 9(3), 222–226.
1055 <https://doi.org/10.1038/ngeo2654>
- 1056 Hondula, K. L., Jones, C. N., & Palmer, M. A. (2021). Effects of seasonal inundation on methane
1057 fluxes from forested freshwater wetlands. *Environmental Research Letters*, 16(8), 084016.
1058 <https://doi.org/10.1088/1748-9326/AC1193>
- 1059 Huttunen, J. T., Alm, J., Liikanen, A., Juutinen, S., Larmola, T., Hammar, T., ... Martikainen, P.
1060 J. (2003). Fluxes of methane, carbon dioxide and nitrous oxide in boreal lakes and potential
1061 anthropogenic effects on the aquatic greenhouse gas emissions. *Chemosphere*, 52, 609–621.

- 1062 [https://doi.org/10.1016/S0045-6535\(03\)00243-1](https://doi.org/10.1016/S0045-6535(03)00243-1)
- 1063 Jansen, J., Thornton, B. F., Cortés, A., Snöäl, J., Wik, M., MacIntyre, S., & Crill, P. M. (2020).
1064 Drivers of diffusive CH₄ emissions from
1065 shallow subarctic lakes on daily to multi-year timescales. *Biogeosciences*, *17*(7), 1911–
1066 1932. <https://doi.org/10.5194/bg-17-1911-2020>
- 1067 Jensen, D., Cavanaugh, K. C., Simard, M., Christensen, A., Rovai, A., & Twilley, R. (2021).
1068 Aboveground biomass distributions and vegetation composition changes in Louisiana's
1069 Wax Lake Delta. *Estuarine, Coastal and Shelf Science*, *250*, 107139.
1070 <https://doi.org/10.1016/j.ecss.2020.107139>
- 1071 Joabsson, A., Christensen, T. R., & Wallén, B. (1999). Vascular plant controls on methane
1072 emissions from northern peatforming wetlands. *Trends in Ecology & Evolution*, *14*(10),
1073 385–388. [https://doi.org/10.1016/S0169-5347\(99\)01649-3](https://doi.org/10.1016/S0169-5347(99)01649-3)
- 1074 Johnston, S. E., Striegl, R. G., Bogard, M. J., Dornblaser, M. M., Butman, D. E., Kellerman, A.
1075 M., ... Spencer, R. G. M. (2020). Hydrologic connectivity determines dissolved organic
1076 matter biogeochemistry in northern high-latitude lakes. *Limnology and Oceanography*
1077 *Oceanography*. <https://doi.org/10.1002/lno.11417>
- 1078 Jordahl, Kelsey, Joris Van den Bossche, Martin Fleischmann, James McBride, Jacob
1079 Wasserman, Adrian Garcia Badaracco, Jeffrey Gerard, Alan D. Snow, Jeff Tratner,
1080 Matthew Perry, Carson Farmer, Geir Arne Hjelle, Micah Cochran, Sean Gillies, Lucas
1081 Culbertson, Matt Bartos, Brendan Ward, Giacomo Caria, Mike Taves, ... Leah Wasser.
1082 (2021). *geopandas/geopandas: v0.10.2 (v0.10.2)*. Zenodo.
1083 <https://doi.org/10.5281/zenodo.5573592>
- 1084 Juutinen, S., Alm, J., Larmola, T., Huttunen, J. T., Morero, M., Martikainen, P. J., & Silvola, J.
1085 (2003). Major implication of the littoral zone for methane release from boreal lakes. *Global*
1086 *Biogeochemical Cycles*, *17*(4). <https://doi.org/10.1029/2003gb002105>
- 1087 Kankaala, P., Huotari, J., Tulonen, T., & Ojala, A. (2013). Lake-size dependent physical forcing
1088 drives carbon dioxide and methane effluxes from lakes in a boreal landscape. *Limnology*
1089 *and Oceanography*, *58*(6), 1915–1930. <https://doi.org/10.4319/lo.2013.58.6.1915>
- 1090 Kankaala, P., Kaki, T., Makela, S., Ojala, A., Pajunen, H., & Arvola, L. (2005). Methane efflux
1091 in relation to plant biomass and sediment characteristics in stands of three common
1092 emergent macrophytes in boreal mesoeutrophic lakes. *Global Change Biology*, *11*(1), 145–
1093 153. <https://doi.org/10.1111/j.1365-2486.2004.00888.x>
- 1094 McKenzie Kuhn, Ruth Varner, David Bastviken, Patrick Crill, Sally MacIntyre, et al. 2021a.
1095 BAWLD-CH₄: Methane Fluxes from Boreal and Arctic Ecosystems. Arctic Data Center.
1096 [doi:10.18739/A2DN3ZX1R](https://doi.org/10.18739/A2DN3ZX1R).
- 1097 Kuhn, M. A., Varner, R. K., Bastviken, D., Crill, P., Macintyre, S., Turetsky, M., Anthony, K.
1098 W., Mcguire, A. D., & Olefeldt, D. (2021b). BAWLD-CH₄ : a comprehensive dataset of
1099 methane fluxes from boreal and arctic ecosystems. *Earth Syst. Sci. Data*, *13*, 5151–5189.

- 1100 <https://doi.org/10.5194/essd-13-5151-2021>
- 1101 Kyzivat, E. D., Smith, L. C., Pitcher, L. H., Arvesen, J., Pavelsky, T. M., Cooley, S. W., & Topp,
1102 S. (2018). ABoVE: AirSWOT Color-Infrared Imagery Over Alaska and Canada, 2017.
1103 ORNL Distributed Active Archive Center. <https://doi.org/10.3334/ORNLDAAAC/1643>
- 1104 Kyzivat, E. D., Smith, L. C., Pitcher, L. H., Fayne, J. V., Cooley, S. W., Cooper, M. G., ...
1105 Pavelsky, T. M. (2019). A high-resolution airborne color-infrared camera water mask for
1106 the NASA ABoVE campaign. *Remote Sensing*, *11*, 1–28.
1107 <https://doi.org/10.3390/rs11182163>
- 1108 Kyzivat, E. D., Smith, L. C., Pitcher, L. H., Fayne, J. V., Cooley, S. W., Cooper, M. G., Topp, S.,
1109 Langhorst, T., Harlan, M. E., Gleason, C. J., & Pavelsky, T. M. (2020). ABoVE: AirSWOT
1110 Water Masks from Color-Infrared Imagery over Alaska and Canada, 2017 (Version 1).
1111 ORNL Distributed Active Archive Center. <https://doi.org/10.3334/ORNLDAAAC/1707>
- 1112 Kyzivat, E. D., Smith, L. C., Huang, C., Wang, C., Langhorst, T., Fayne, J. V., Harlan, M.E.,
1113 Ishitsuka, Y., Feng, D., Dolan, W., Pitcher, L.H, Pavelsky, T. M. (2021a). ABoVE: Lake
1114 and Wetland Classification from L-band SAR, Alaska and Canada, 2017-2019. ORNL
1115 Distributed Active Archive Center. <https://doi.org/10.3334/ORNLDAAAC/1883>
- 1116 Kyzivat, E., F. Garcia Tigreros, T. Langhorst, J.V. Fayne, M.E. Harlan, Y. Ishitsuka, D. Feng,
1117 K.P. Wickland, M.M. Dornblaser, R.G. Striegl, D.E. Butman, and C.J. Gleason. 2021b.
1118 Methane and carbon dioxide fluxes from vegetated and open water zones of lakes in the
1119 Peace-Athabasca Delta, Alberta, Canada, 2019 ver 1. Environmental Data Initiative.
1120 <https://doi.org/10.6073/pasta/1e0cadadd8024c8fabcb692ee21dc1f57> (Accessed 2022-03-04).
- 1121 Laanbroek, H. J. (2009). Methane emission from natural wetlands: interplay between emergent
1122 macrophytes and soil microbial processes. A mini-review.
- 1123 Langenegger, T., Vachon, D., Donis, D., & McGinnis, D. F. (2019). What the bubble knows:
1124 Lake methane dynamics revealed by sediment gas bubble composition. *Limnology and*
1125 *Oceanography*, *64*(4), 1526–1544. <https://doi.org/10.1002/LNO.11133>
- 1126 Larmola, T., Alm, J., Juutinen, S., Huttunen, J. T., Martikainen, P. J., & Silvola, J. (2004).
1127 Contribution of vegetated littoral zone to winter fluxes of carbon dioxide and methane from
1128 boreal lakes. *J. Geophys. Res*, *109*. <https://doi.org/10.1029/2004JD004875>
- 1129 Lehner, B., & Döll, P. (2004). Development and validation of a global database of lakes,
1130 reservoirs and wetlands. *Journal of Hydrology*, *296*, 1–22.
1131 <https://doi.org/10.1016/j.jhydrol.2004.03.028>
- 1132 Li, M., Peng, C., Zhu, Q., Zhou, X., Yang, G., Song, X., & Zhang, K. (2020). The significant
1133 contribution of lake depth in regulating global lake diffusive methane emissions. *Water*
1134 *Research*, *172*, 115465. <https://doi.org/10.1016/j.watres.2020.115465>
- 1135 Loken, L. C., Crawford, J. T., Schramm, P. J., Stadler, P., Desai, A. R., & Stanley, E. H. (2019).
1136 Large Spatial and Temporal Variability of Carbon Dioxide and Methane in a Eutrophic

- 1137 Lake. *Journal of Geophysical Research: Biogeosciences*, 124(7), 2248–2266.
1138 <https://doi.org/10.1029/2019JG005186>
- 1139 Mäkelä, S., Huitu, E., & Arvola, L. (2004). Spatial patterns in aquatic vegetation composition
1140 and environmental covariates along chains of lakes in the Kokemäenjoki watershed (S.
1141 Finland). *Aquatic Botany*, 80(4), 253–269. <https://doi.org/10.1016/j.aquabot.2004.08.006>
- 1142 Melton, J. R., Wania, R., Hodson, E. L., Poulter, B., Ringeval, B., Spahni, R., ... Kaplan, J. O.
1143 (2013). Present state of global wetland extent and wetland methane modelling: conclusions
1144 from a model inter-comparison project (WETCHIMP). *Biogeosciences*, 10, 753–788.
1145 <https://doi.org/10.5194/bg-10-753-2013>
- 1146 Messenger, M. L., Lehner, B., Grill, G., Nedeva, I., & Schmitt, O. (2016). Estimating the volume
1147 and age of water stored in global lakes using a geo-statistical approach. *Nature*
1148 *Communications*, 7, 1–11. <https://doi.org/10.1038/ncomms13603>
- 1149 Michmerhuizen, C. M., Striegl, R. G., & McDonald, M. E. (1996). Potential methane emission
1150 from north-temperate lakes following ice melt. *Limnology and Oceanography*, 41(5), 985–
1151 991. <https://doi.org/10.4319/lo.1996.41.5.0985>
- 1152 Miller, C., Griffith, C. P., Goetz, S. J., Hoy, E. E., Pinto, N., McCubbin, I. B., ... Margolis, H. A.
1153 (2019). An overview of ABoVE airborne campaign data acquisitions and science
1154 opportunities. *Environmental Research Letters*, 14(8). <https://doi.org/10.1088/1748-9326/ab0d44>
- 1156 NASA/JPL. (2017-2019). UAVSAR_POLSAR [Data set]. NASA Alaska Satellite Facility
1157 DAAC. <https://doi.org/10.5067/7PEQV8SVR4DM>
- 1158 Natchimuthu, S., Sundgren, I., Gålfalk, M., Klemedtsson, L., Crill, P., Danielsson, Å., &
1159 Bastviken, D. (2016). Spatio-temporal variability of lake CH₄ fluxes and its influence on
1160 annual whole lake emission estimates. *Limnology and Oceanography*, 61(S1), S13–S26.
1161 <https://doi.org/10.1002/lno.10222>
- 1162 Nelson, S. A. C., Cheruvilil, K. S., & Soranno, P. A. (2006). Satellite remote sensing of
1163 freshwater macrophytes and the influence of water clarity. *Aquatic Botany*, 85(4), 289–298.
1164 <https://doi.org/10.1016/j.aquabot.2006.06.003>
- 1165 David Olefeldt, Mikael Hovemyr, McKenzie Kuhn, David Bastviken, Theodore Bohn, et al.
1166 2021. The fractional land cover estimates from the Boreal-Arctic Wetland and Lake Dataset
1167 (BAWLD), 2021b. Arctic Data Center. <https://doi.org/10.18739/A2C824F9X>
- 1168 Olefeldt, D., Hovemyr, M., Kuhn, M. A., Bastviken, D., Bohn, T. J., Connolly, J., Crill, P.,
1169 Euskirchen, E. S., Finkelstein, S. A., Genet, H., Grosse, G., Harris, L. I., Heffernan, L.,
1170 Helbig, M., Hugelius, G., Hutchins, R., Juutinen, S., Lara, M. J., Malhotra, A., ... Watts, J.
1171 D. (2021a). The Boreal-Arctic Wetland and Lake Dataset (BAWLD) D. Olefeldt et al.: The
1172 Boreal-Arctic Wetland and Lake Dataset. *Earth Syst. Sci. Data*, 13, 5127–5149.
1173 <https://doi.org/10.5194/essd-13-5127-2021>

- 1174 Parks Canada. (2019). *Wood Buffalo National Park World Heritage Site Action Plan* (Cat. No.:
1175 978-0-660-27537-6). Retrieved from [https://pcacdn.azureedge.net/-/media/pn-
np/nt/woodbuffalo/2021-changes/02_11-action-plan-PDFs/WoodBuffalo-WHS-Action-
Plan_EN.pdf](https://pcacdn.azureedge.net/-/media/pn-
1176 np/nt/woodbuffalo/2021-changes/02_11-action-plan-PDFs/WoodBuffalo-WHS-Action-
1177 Plan_EN.pdf)
- 1178 Pavelsky, T. M., & Smith, L. C. (2008). Remote sensing of hydrologic recharge in the Peace-
1179 Athabasca Delta, Canada. *Geophysical Research Letters*.
1180 <https://doi.org/10.1029/2008GL033268>
- 1181 Rey-Sanchez, A. C., Morin, T. H., Stefanik, K. C., Wrighton, K., & Bohrer, G. (2018).
1182 Determining total emissions and environmental drivers of methane flux in a Lake Erie
1183 estuarine marsh. *Ecological Engineering*, *114*, 7–15.
1184 <https://doi.org/10.1016/j.ecoleng.2017.06.042>
- 1185 Ribaudo, C., Bartoli, M., Longhi, D., Castaldi, S., Neubauer, S. C., & Viaroli, P. (2012). CO₂
1186 and CH₄ fluxes across a *Nuphar lutea* (L.) Sm. stand. *Journal of Limnology*, *71*(1), 200–
1187 210.
- 1188 Rosentreter, J. A., Borges, A. v., Deemer, B. R., Holgerson, M. A., Liu, S., Song, C., Melack, J.,
1189 Raymond, P. A., Duarte, C. M., Allen, G. H., Olefeldt, D., Poulter, B., Battin, T. I., & Eyre,
1190 B. D. (2021). Half of global methane emissions come from highly variable aquatic
1191 ecosystem sources. *Nature Geoscience*. <https://doi.org/10.1038/s41561-021-00715-2>
- 1192 Saunio, M., Stavert, A. R., Poulter, B., Bousquet, P., Canadell, J. G., Jackson, R. B., ... Zhuang,
1193 Q. (2020). The Global Methane Budget 2000–2017. *Earth Syst. Sci. Data*, *12*, 1561–1623.
1194 <https://doi.org/10.5194/essd-12-1561-2020>
- 1195 Schmiedeskamp, M., Stephanie, L., Praetzel, E., Bastviken, D., & Knorr, K.-H. (2021). Whole-
1196 lake methane emissions from two temperate shallow lakes with fluctuating water levels:
1197 Relevance of spatiotemporal patterns. *Limnol. Oceanogr*, *9999*, 1–15.
1198 <https://doi.org/10.1002/lno.11764>
- 1199 Seekell, D., Cael, B., Norman, S., & Byström, P. (2021). Patterns and Variation of Littoral
1200 Habitat Size Among Lakes. *Geophysical Research Letters*, *48*(20), e2021GL095046.
1201 <https://doi.org/10.1029/2021GL095046>
- 1202 Simard, M., Riel, B. V., Denbina, M., & Hensley, S. (2016). Radiometric Correction of Airborne
1203 Radar Images over Forested Terrain with Topography. *IEEE Transactions on Geoscience
1204 and Remote Sensing*, *54*(8), 4488–4500. <https://doi.org/10.1109/TGRS.2016.2543142>
- 1205 Slaymaker, O. (2016). *Landscapes and Landforms of Western Canada*. Springer International
1206 Publishing.
- 1207 Smith, L. K., & Lewis, W. M. (1992). Seasonality of methane emissions from five lakes and
1208 associated wetlands of the Colorado Rockies. *Global Biogeochemical Cycles*, *6*(4), 323–
1209 338. <https://doi.org/10.1029/92GB02016>
- 1210 Smith, V. H., & Wallsten, M. (1986). Prediction of emergent and floating-leaved macrophyte

- 1211 cover in Central Swedish lakes. *Canadian Journal of Fisheries and Aquatic Sciences*,
1212 43(12), 2519–2523. <https://doi.org/10.1139/f86-311>
- 1213 Spence, C., & Woo, M. (2006). Hydrology of subarctic Canadian Shield: heterogeneous
1214 headwater basins. *Journal of Hydrology*, 317(1–2), 138–154.
1215 <https://doi.org/10.1016/J.JHYDROL.2005.05.014>
- 1216 Stephanie, L., Praetzel, E., Plenter, N., Schilling, S., Schmiedeskamp, M., Broll, G., ...
1217 Praetzel@uni-Muenster, L. De. (2020). Organic matter and sediment properties determine
1218 in-lake variability of sediment CO₂ and CH₄ production and emissions of a small and
1219 shallow lake. *Biogeosciences*, 17, 5057–5078. <https://doi.org/10.5194/bg-17-5057-2020>
- 1220 Striegl, R. G., Dornblaser, M. M., McDonald, C. P., Rover, J. R., & Stets, E. G. (2012). Carbon
1221 dioxide and methane emissions from the Yukon River system. *Global Biogeochemical*
1222 *Cycles*, 26(4). <https://doi.org/10.1029/2012GB004306>
- 1223 Striegl, R. G., & Michmerhuizen, C. M. (1998). Hydrologic influence on methane and carbon
1224 dioxide dynamics at two north-central Minnesota lakes. *Limnology and Oceanography*,
1225 43(7), 1519–1529. <https://doi.org/10.4319/lo.1998.43.7.1519>
- 1226 Ström, L., Mastepanov, M., & Christensen, T. R. (2005). Species-specific Effects of Vascular
1227 Plants on Carbon Turnover and Methane Emissions from Wetlands. *Biogeochemistry*,
1228 75(1), 65–82. <https://doi.org/10.1007/s10533-004-6124-1>
- 1229 Thornton, B. F., Wik, M., & Crill, P. M. (2016). Double-counting challenges the accuracy of
1230 high-latitude methane inventories. *Geophysical Research Letters*, 43(24), 12,569–12,577.
1231 <https://doi.org/10.1002/2016GL071772>
- 1232 Timoney, K. P. (2013). *The Peace-Athabasca Delta: Portrait of a Dynamic Ecosystem*.
1233 Edmonton: University of Alberta Press.
- 1234 Töyrä, J., & Pietroniro, A. (2005). Towards operational monitoring of a northern wetland using
1235 geomatics-based techniques. *Remote Sensing of Environment*, 97(2), 174–191.
1236 <https://doi.org/10.1016/J.RSE.2005.03.012>
- 1237 Tranvik, L. J., Downing, J. A., Cotner, J. B., Loiselle, S. A., Striegl, R. G., Ballatore, T. J., ...
1238 Weyhenmeyer, G. A. (2009). Lakes and reservoirs as regulators of carbon cycling and
1239 climate. *Limnology and Oceanography*, 54(6part2), 2298–2314.
1240 https://doi.org/10.4319/lo.2009.54.6_part_2.2298
- 1241 Ulander, L. M. H. (1996). Radiometric slope correction of synthetic-aperture radar images. *IEEE*
1242 *Transactions on Geoscience and Remote Sensing*, 34(5), 1115–1122.
1243 <https://doi.org/10.1109/36.536527>
- 1244 Verpoorter, C., Kutser, T., Seekell, D. A., & Tranvik, L. J. (2014). A global inventory of lakes
1245 based on high-resolution satellite imagery. *Geophysical Research Letters*, 41(18), 6396–
1246 6402. <https://doi.org/10.1002/2014GL060641>

- 1247 Villa, J. A., Ju, Y., Yazbeck, T., Waldo, S., Wrighton, K. C., & Bohrer, G. (2021). Ebullition
1248 dominates methane fluxes from the water surface across different ecohydrological patches
1249 in a temperate freshwater marsh at the end of the growing season. *Science of the Total*
1250 *Environment*, 767, 144498. <https://doi.org/10.1016/j.scitotenv.2020.144498>
- 1251 Wang, J. A., Sulla-menashe, D., Woodcock, C. E., Sonnentag, O., Keeling, R. F., & Friedl, M.
1252 A. (2019). ABoVE: Landsat-derived Annual Dominant Land Cover Across ABoVE Core
1253 Domain, 1984-2014. ORNL Distributed Active Archive Center.
1254 <https://doi.org/10.3334/ORNLDAAAC/1691>
- 1255 Wang, J. A., Sulla-Menashe, D., Woodcock, C. E., Sonnentag, O., Keeling, R. F., & Friedl, M.
1256 A. (2019). Extensive land cover change across Arctic–Boreal Northwestern North America
1257 from disturbance and climate forcing. *Global Change Biology*, 00, 1–16.
1258 <https://doi.org/10.1111/gcb.14804>
- 1259 Ward, E. M., & Gorelick, S. M. (2018). Drying drives decline in muskrat population in the
1260 Peace-Athabasca Delta, Canada. *Environmental Research Letters*, 13, 124026.
1261 <https://doi.org/10.1088/1748-9326/aaf0ec>
- 1262 West, W. E., Creamer, K. P., & Jones, S. E. (2016). Productivity and depth regulate lake
1263 contributions to atmospheric methane. *Limnology and Oceanography*, 61(S1), S51–S61.
1264 <https://doi.org/10.1002/LNO.10247>
- 1265 Wetzel, R. G. (1990). Land-water interfaces: Metabolic and limnological regulators. *Verh.*
1266 *Internat. Verein. Limnol.*, 24(September), 6–24.
- 1267 Wetzel, R. G. (2001). *Limnology: Lake and River Ecosystems* (Third). Boston: Academic Press.
- 1268 Wik, M., Crill, P. M., Varner, R. K., & Bastviken, D. (2013). Multiyear measurements of
1269 ebullitive methane flux from three subarctic lakes. *Journal of Geophysical Research:*
1270 *Biogeosciences*, 118(3), 1307–1321. <https://doi.org/10.1002/jgrg.20103>
- 1271 Wik, M., Varner, R. K., Anthony, K. W., MacIntyre, S., & Bastviken, D. (2016a). Climate-
1272 sensitive northern lakes and ponds are critical components of methane release. *Nature*
1273 *Geoscience*, 9(2), 99–105. <https://doi.org/10.1038/ngeo2578>
- 1274 Wik, M., Thornton, B. F., Bastviken, D., Uhlbäck, J., & Crill, P. M. (2016b). Biased sampling of
1275 methane release from northern lakes: A problem for extrapolation. *Geophysical Research*
1276 *Letters*, 43(3), 1256–1262. <https://doi.org/10.1002/2015GL066501>
- 1277 Wolfe, B. B., Hall, R. I., Last, W. M., Edwards, T. W. D., English, M. C., Karst-Riddoch, T. L.,
1278 ... Palmi, R. (2006). Reconstruction of multi-century flood histories from oxbow lake
1279 sediments, Peace-Athabasca Delta, Canada. *Hydrological Processes*, 20(19), 4131–4153.
1280 <https://doi.org/10.1002/hyp.6423>
- 1281 Zhang, B., Tian, H., Lu, C., Chen, G., Pan, S., Anderson, C., & Poulter, B. (2017). Methane
1282 emissions from global wetlands: An assessment of the uncertainty associated with various
1283 wetland extent data sets. *Atmospheric Environment*, 165, 310–321.

- 1284 <https://doi.org/10.1016/J.ATMOSENV.2017.07.001>
- 1285 Zhang, S., Foerster, S., Medeiros, P., de Araújo, J. C., & Waske, B. (2018). Effective water
1286 surface mapping in macrophyte-covered reservoirs in NE Brazil based on TerraSAR-X time
1287 series. *International Journal of Applied Earth Observation and Geoinformation*, *69*, 41–55.
1288 <https://doi.org/10.1016/j.jag.2018.02.014>
- 1289 Zhang, Y., Jeppesen, E., Liu, X., Qin, B., Shi, K., Zhou, Y., ... Deng, J. (2017). Global loss of
1290 aquatic vegetation in lakes. *Earth-Science Reviews*, *173*, 259–265.
1291 <https://doi.org/https://doi.org/10.1016/j.earscirev.2017.08.013>
- 1292 Zhang, Z., Ni, W., Sun, G., Huang, W., Ranson, K. J., Cook, B. D., & Guo, Z. (2017). Biomass
1293 retrieval from L-band polarimetric UAVSAR backscatter and PRISM stereo imagery.
1294 *Remote Sensing of Environment*, *194*, 331–346. <https://doi.org/10.1016/J.RSE.2017.03.034>
- 1295 Zhang, Z., Fluet-Chouinard, E., Jensen, K., Mcdonald, K., Hugelius, G., Gumbricht, T., ...
1296 Poulter, B. (2021). Development of the global dataset of Wetland Area and Dynamics for
1297 Methane Modeling (WAD2M). *Earth Syst. Sci. Data*, *13*. [https://doi.org/10.5194/essd-13-](https://doi.org/10.5194/essd-13-2001-2021)
1298 [2001-2021](https://doi.org/10.5194/essd-13-2001-2021)
- 1299